Electronic Supplementary Material (ESI) for Chemical Science.

Substituents converting the molecular luminescence from thermally activated delayed fluorescence to ultralong room-temperature phosphorescence

Zetong Ma, Zhiqiang Yang, Lan Mu, Lisong Deng, Liangjian Chen, Bohan Wang, Xianfeng Qiao, Dehua Hu,* Bing Yang, Dongge Ma, Junbiao Peng and Yuguang Ma*

Materials and Measurements

^{1}H NMR, ^{13}C NMR spectra were recorded in deuterated solvents on a Bruker AVANCE 400 MHz NMR Spectrometer. ^{1}H NMR and ^{13}C NMR chemical shifts are reported in ppm downfield from tetramethylsilane (TMS) reference using the residual protonated solvent as an internal standard. Mass spectra were determined on Waters ACQUITY TOD Mass Spectrometer.

Absorption spectra were measured with Shimadzu (UV-3600) UV-Vis-NIR spectrophotometer in a 1-cm quartz cell. Thermal gravity analysis (TGA) spectra were measured with NETZSCH TG 209 F3 Tarsus while differential scanning calorimetry (DSC) spectra were recorded on NETZSCH DSC 200 F3 Maia. Emission spectra were measured with SHIMADZU RF-5301pc or Edinburgh FLS980 or Horiba Fluoromax4 Spectrofluorometer. The absolute photoluminescence quantum yields of fluorescence were collected by HAMAMATSU Quantaurus-QY instrument in air. As for the PLQYs of phosphorescence, they were obtained according to the intensity proportion of the phosphorescent part to the total luminescence and the total luminescence quantum yield at the steady state. The integral area of fluorescence, phosphorescence and total luminescence were used as primary data. The data of transient fluorescence/phosphorescence decay spectra were determined with HAMAMATSU Quantaurus-Tau spectrometer C11367 or Edinburgh FLS980 spectrometer. Cyclic voltammetry (CV) was performed with a CHI620E electrochemical workstation using glassy carbon discs as the working electrode, Pt wire as the counter electrode, Ag/AgCl electrode as the reference electrode at a scanning rate of 100 mV/s. 0.1 M tetrabutylammonium hexafluorophosphate ($TBAPF_6$) dissolved in CH_2Cl_2 or DMF was employed as the supporting electrolyte. The plot includes the signal of the ferrocene as an internal potential marker. CH_2Cl_2 and DMF were freshly distilled prior to use. Single crystals data collections were performed on XtaLAB P200 FR-X diffractometer, using Mo Kα radiation (0.71073 Å). Using Olex2, these structures were solved with the ShelXS and refined with the ShelXL-2014 refinement package using Least Squares minimization. Refinement was performed on F^2 anisotropically for all the non-hydrogen atoms by the full-matrix least-squares method. The hydrogen atoms were placed at the calculated positions and were included in the structure calculation without further refinement of the parameters.

All chemicals were purchased from commercial suppliers (for example, J&K Corp.) and used without further purification unless otherwise specified.

Synthesis and Characterization

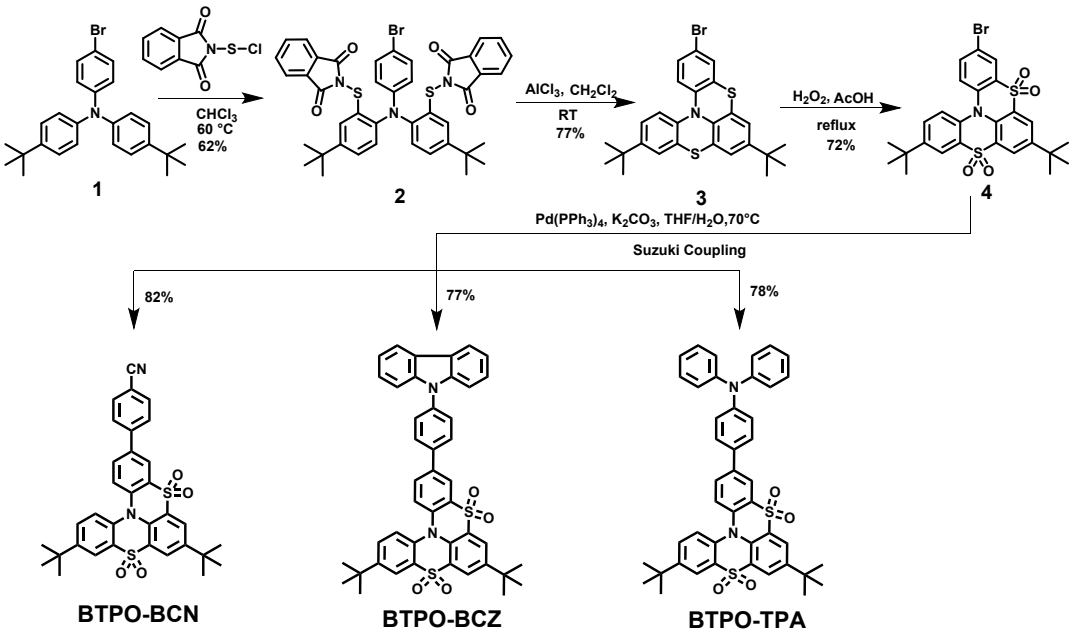

Scheme S1. The synthetic routes towards benzo[5,6][1,4]thiazino[2,3,4-kl]phenothiazine 5,5,9,9-tetraoxide (BTPO) derivates.

The starting material compound 1 and phthalimidesulfenyl chloride (PhtNSCl) was synthesized according to the previous literatures[1].

(1) Compound 2:

To a solution of 4-bromo-N,N-bis(4-(tert-butyl)phenyl)aniline (1) (3 mmol, 1.31 g)in dry chloroform (60 mL) was added PhtNSCl (7.5 mmol, 1.60 g) under Ar atmosphere. The mixture was further stirring at 60 ℃ for 24 hours. Then the reaction solution was diluted with DCM, and was washed with a saturated $NaHCO_3$ solution and water twice. The organic layer was further dried with Na_2SO_4 and concentrated under reduced pressure, and then purified by column chromatography on silica gel with CH_2Cl_2/petroleum ether (4:1) to give compound 2 as light-yellow solid (62% yield, 1.471 g). ^{1}H NMR (400 MHz, Chloroform-d) δ 7.94 (dd, J = 5.5, 3.0 Hz, 4H), 7.80 (dd, J = 5.5, 3.1 Hz, 4H), 7.71 (d, J = 8.4 Hz, 2H), 7.33 (dd, J = 8.4, 2.2 Hz, 2H), 7.31 – 7.27 (m, 2H), 7.19 (d, J = 2.2 Hz, 2H), 6.63 – 6.54 (m, 2H), 1.17 (s, 18H). ^{13}C NMR (126 MHz, $CDCl_3$) δ 167.91, 150.22, 147.87, 141.04, 134.77, 133.12, 132.73, 131.95, 129.16, 126.88, 124.67, 124.00, 118.61, 112.61, 34.57, 31.08. MALDI-TOF MS (mass m/z): calcd for $C_{42}H_{36}BrN_3O_4S_2Na^+$: 812.1223, found 812.3427 [MNa+].

(2) Compound 3:

To a solution of compound 2 (1.5 mmol, 1.19 g) in dry DCM (60 mL) was added $AlCl_3$ (6 mmol, 1 g) under Ar atmosphere. The reaction mixture was stirred at room temperature and monitored by TLC. After the starting materials was disappeared, the mixture was diluted by DCM, and washed with a saturated $NaCO_3$ and water twice. The organic layer was further dried with Na_2SO_4 and concentrated under reduced pressure, and then purified by column chromatography on silica gel with petroleum ether to affored compound 3 as yellow solid (77% yield, 0.65 g). ^{1}H NMR (400 MHz, Chloroform-d) δ 7.32 (d, J = 2.2 Hz, 1H), 7.21 (d, J = 2.2 Hz, 1H), 7.16 (m, 3H), 7.12 – 7.02 (m, 3H), 7.01 (d, J = 2.0 Hz, 1H), 6.96 (d, J = 2.1 Hz, 1H), 1.30 (s, 9H), 1.25 (s, 9H). ^{13}C NMR (126 MHz, $CDCl_3$) δ 129.92, 124.52, 122.84, 122.57, 34.25, 31.42, 31.27, 29.68, 1.00. MALDI-TOF MS (mass m/z): calcd for $C_{26}H_{26}BrNS_2$: 495.0690, found 495.2247 [M$^+$].

(3) Compound 4:

Compound 3 (1.15 mmol, 571mg) dissolved in AcOH (25 mL) was added 1.5 mL H_2O_2. The reaction mixture was heated at 100 ℃ for 4 hours. Quenched with 100 mL water, the precipitate was collected by filtration. Then the crude product was further purified by column chromatography on silica gel with DCM/peteroleum ether (2:1) to give compound 4 as a white solid (72% yield, 465 mg). ^{1}H NMR (400 MHz, Chloroform-d) δ 8.34 (d, J = 2.2 Hz, 1H), 8.30 (d, J = 2.2 Hz, 1H), 8.29 (d, J = 2.3 Hz, 1H), 8.15 (d, J = 2.3 Hz, 1H), 7.69 (dd, J = 8.9, 2.3 Hz, 1H), 7.64 (dd, J = 8.7, 2.3 Hz, 1H), 7.56 (dd, J = 8.8, 7.2 Hz, 2H), 1.43 (s, 9H), 1.39 (s, 9H). ^{13}C NMR (126 MHz, $CDCl_3$) δ 150.57, 150.47, 149.57, 138.42, 136.59, 136.32, 134.63, 131.08, 130.55, 129.25, 128.93, 128.39, 126.89, 124.91, 124.56, 123.56, 121.70, 120.67, 118.71, 35.58, 35.18, 31.09. APCI (mass m/z): calcd for $C_{26}H_{26}BrNO_4S_2$: 559.05, found 559.51 [M$^+$].

(4) General procedure for the Suzuki coupling:

The schlenk flask was charged with compound 4 (1.43 mmol, 800 mg), respective boronic acid ester (4-(4,4,5,5-tetramethyl-1,3,2-dioxaborolan-2-yl)benzonitrile, 9-(4-(4,4,5,5-tetramethyl-1,3,2-dioxaborolan-2-yl)phenyl)-9H-carbazole, N,N-diphenyl-4-(4,4,5,5-tetramethyl-1,3,2-dioxaborolan-2-yl)aniline and 4,4,5,5-tetramethyl-2-phenyl-1,3,2-dioxaborolane) (1.3 equivalent, 1.86 mmol), K_2CO_3 (2.14 mmol, 296 mg) and THF/water (5:1 v/v, 40 mL/8 mL). After degassed by Ar, the mixture was added $Pd(PPh_3)_4$ and stirred at 78 ℃ for 24 hours. The reaction mixture was quenched by water and extracted by DCM. Dried over $MgSO_4$ and concentrated under reduced pressure, the residue was further purified by column chromatography on silica gel to afford respective target product.

BTPO-BCN:

White solid (82% yield, 685mg). ^{1}H NMR (500 MHz, Chloroform-d) δ 8.38 (s, 1H), 8.36 (d, J = 2.1 Hz, 1H), 8.34 (d, J = 2.1 Hz, 1H), 8.18 (d, J = 1.8 Hz, 1H), 7.81 – 7.80 (m, 4H), 7.75 – 7.74 (m, 2H), 7.67 (m, 1H), 7.63 (m, 1H), 1.44 (s, 9H), 1.41 (s, 9H). ^{13}C NMR (126 MHz, $CDCl_3$) δ 150.62, 149.62, 142.50, 139.41, 137.05, 136.67, 134.71, 133.02, 131.77, 131.04, 129.91, 129.31, 128.93, 128.44, 127.63, 124.87, 124.57, 122.76, 122.68, 121.89, 120.69, 118.41, 112.25, 35.59, 35.20, 31.10. MALDI-TOF MS (mass m/z): calcd for $C_{33}H_{30}N_2O_4S_2$:582.1647, found 582.5804 [M$^+$].

BTPO-BCZ:

White solid (77%, 797 mg). ^{1}H NMR (500 MHz, Chloroform-d) δ 8.48 (d, J = 2.1 Hz, 1H), 8.37 (s, 2H), 8.19 (m, 1H), 8.17 (d, J = 7.7 Hz, 2H), 7.91 (dd, J = 8.6, 2.2 Hz, 1H), 7.89 – 7.87 (m, 2H), 7.83 (d, J = 8.6 Hz, 1H), 7.74 – 7.72 (m, 2H), 7.69 (m, 2H), 7.51 – 7.49 (m, 2H), 7.46 – 7.43 (m, 2H), 7.34 – 7.31 (m, 2H), 1.45 (s, 9H), 1.42 (s, 9H). ^{13}C NMR (126 MHz, $CDCl_3$) δ 150.37, 149.39, 140.64, 138.57, 138.41, 138.11, 137.10, 136.86, 134.82, 131.74, 131.02, 129.83, 129.15, 128.81, 128.54, 128.46, 127.68, 126.08, 124.76, 124.60, 123.57, 122.65, 122.29, 121.93, 120.60, 120.41, 120.23, 109.74, 35.59, 35.19, 31.14. MALDI-TOF MS (mass m/z): calcd for $C_{44}H_{38}NO_4S_2$: 722.2273, found 722.4406 [M$^+$].

BTPO-TPA:

Yellow solid (78% yield, 811 mg). ^{1}H NMR (500 MHz, Chloroform-d) δ 8.35 – 8.33 (m, 2H), 8.33 (d, J = 2 Hz, 1H), 8.16 (s , 1H), 7.77 (dd, J = 8.7, 2.1 Hz, 1H), 7.71 (d, J = 8.7 Hz, 1H), 7.65 (s, 2H), 7.50 – 7.48 (m, 2H), 7.32 – 7.28 (m, 4H), 7.16 – 7.15 (m, 6H), 7.08 (t, J = 7.3, 2H), 1.43 (s, 9H), 1.40 (s, 9H). ^{13}C NMR (126 MHz, $CDCl_3$) δ 150.12, 149.15, 148.37, 147.30, 139.02, 137.61, 136.92, 134.81, 131.36, 131.16, 130.95, 129.66, 129.42, 128.94, 128.64, 128.52, 127.64, 124.89, 124.63, 124.55, 123.51, 123.22, 122.45, 121.88, 121.41, 120.47, 35.55, 35.14, 31.12. MALDI-TOF MS (mass m/z): calcd for $C_{44}H_{40}NO_4S_2$: 724.2429, found 724.4480 [M$^+$].

BTPO-Ph:

White solid (71% yield). ^{1}H NMR (500 MHz, Methylene Chloride-d_2) δ 8.37 (d, *J* = 2.1 Hz, 1H), 8.34 (s, 2H), 8.15 (d, *J* = 2.2 Hz, 1H), 7.87 (dd, *J* = 8.6, 2.2 Hz, 1H), 7.77 (d, *J* = 8.7 Hz, 1H), 7.71 (dd, *J* = 8.8, 2.2 Hz, 1H), 7.69 – 7.64 (m, 3H), 7.55 – 7.48 (m, 2H), 7.47 – 7.40 (m, 1H), 1.44 (s, 9H), 1.41 (s, 9H).^{13}C NMR (126 MHz, CD_2Cl_2) δ 150.84, 149.87, 139.85, 138.90, 138.87, 137.45, 135.36, 132.50, 131.75, 130.40, 129.74, 129.72, 129.51, 129.26, 128.98, 127.55, 125.09, 124.96, 123.02, 122.50, 122.41, 120.82, 36.03, 35.62, 31.40. APCI (mass m/z): calcd for $C_{32}H_{31}NO_4S_2$: 557.2, found 557.8 [M$^+$].

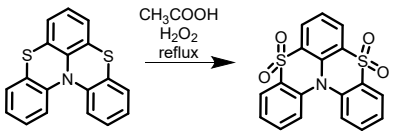

BTP **BTPO**

Scheme S2. The synthetic routes towards benzo[5,6][1,4]thiazino[2,3,4-kl]phenothiazine 5,5,9,9-tetraoxide (BTPO).

(5) BTPO:

The starting material Benzo[5,6][1,4]thiazino[2,3,4-kl]phenothiazine (BTP) was synthesized according to the previous report[2]. 2 mL H_2O_2 was added to the solution of BTP (2.62 mmol ,800 mg) in 30 mL AcOH. The reaction mixture was heated at 100 ℃ for 3 hours. Quenched with 100 mL water, the precipitate was collected by filtration. The target product was obtained from recrystallization from CH_2Cl_2/CH_3OH mixed solution as a white solid (91% yield, 968 mg) .^{1}H NMR (400 MHz, Chloroform-d) δ 8.36 (d, J = 7.8 Hz, 2H), 8.19 (dd, J = 7.8, 1.5 Hz, 2H), 7.73 – 7.66 (m, 3H), 7.63 (ddd, J = 8.4, 7.1, 1.6 Hz, 2H), 7.53 (ddd, J = 8.3, 7.2, 1.3 Hz, 2H). ^{13}C NMR (101

MHz, $CDCl_3$) δ 139.48, 137.08, 133.55, 129.76, 129.18, 127.84, 126.40, 124.92, 124.35, 122.29. APCI (mass m/z): calcd for $C_{18}H_{11}BrNO_4S_2$: 369.01, found 369.32 [M^+].

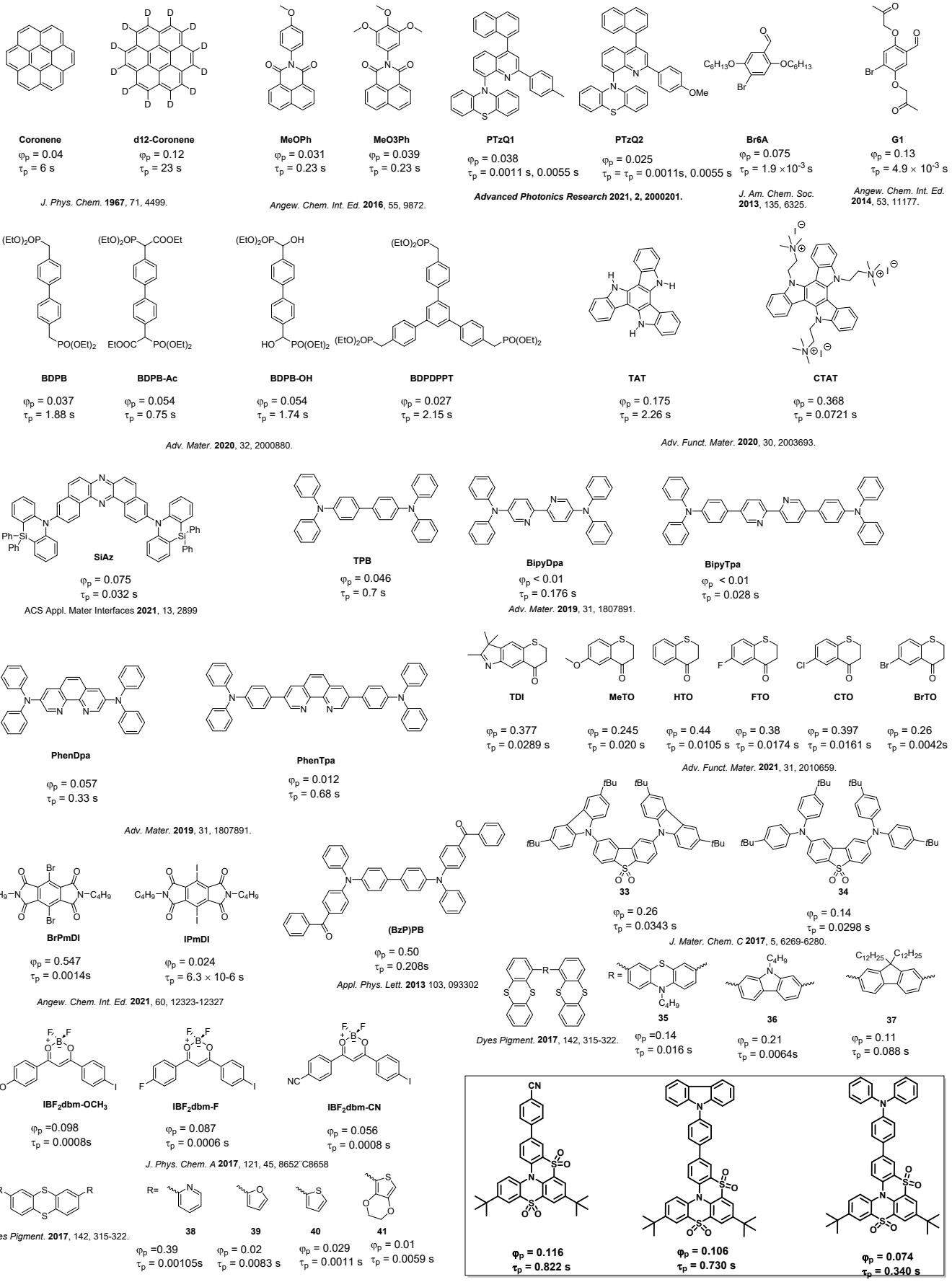

Scheme S3. Molecular structure of reported RTP materials doped in polymer matrix with phosphorescence quantum yield and lifetime.

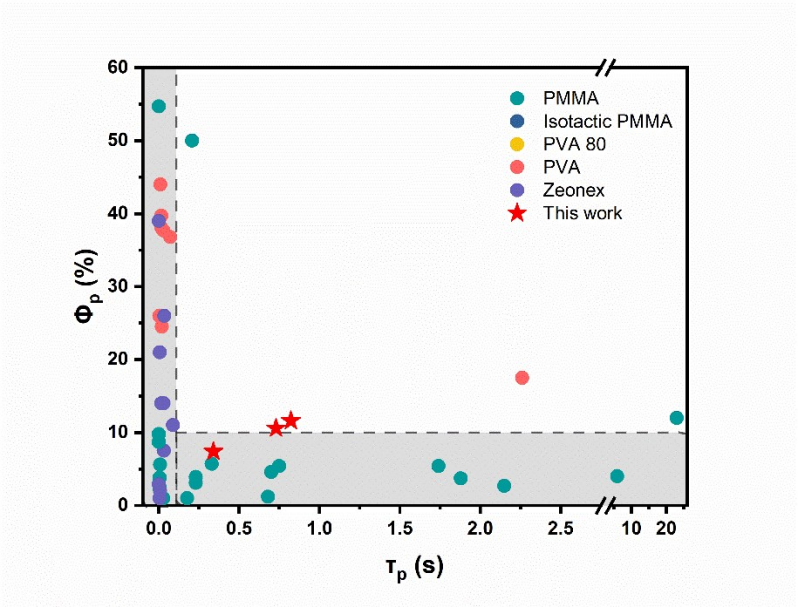

Figure S1. Distribution showing the relationship between RTP lifetime and quantum efficiency of reported monomeric RTP materials doped in different polymer matrix.

Table S1 Phosphorescence properties of reported RTP materials doped in polymer matrix.

NO.	GUEST	HOST	Φ_P (%)	T_P (S)	REFERENCE
1	Coronene	PMMA	4	6	*J. Phys. Chem.* **1967**, 71, 4499.
2	d_{12}-Coronene	PMMA	12	23	*J. Phys. Chem.* **1967**, 71, 4499.
3	MeOPh	PMMA	3.1	0.23	*Angew. Chem. Int. Ed.* **2016**, 55, 9872.
4	MeO3Ph	PMMA	3.9	0.23	*Angew. Chem. Int. Ed.* **2016**, 55, 9872
5	Br6A	Isotactic PMMA	7.5	1.90×10^{-3}	*J. Am. Chem. Soc.* **2013**, 135, 6325.
6	G1	PVA 80	13	4.90×10^{-3}	*Angew. Chem. Int. Ed.***2014**, 53, 11177.
7	BDPB	PMMA	3.7	1.88	*Adv. Mater.* **2020**, 32, 2000880.
8	BDPB-Ac	PMMA	5.4	0.75	*Adv. Mater.* **2020**, 32, 2000880
9	BDPB-OH	PMMA	5.4	1.74	*Adv. Mater.* **2020**, 32, 2000880
10	BDPDPPT	PMMA	2.7	2.15	*Adv. Mater.* **2020**, 32, 2000880
11	TAT	PVA	17.5	2.26	*Adv. Funct. Mater.* **2020**, 30, 2003693.
12	CTAT	PVA	36.8	0.0721	*Adv. Funct. Mater.* **2020**, 30, 2003693.
13	SiAz	Zeonex	7.5	0.032	*ACS Appl. Mater Interfaces* **2021**, 13, 2899
14	TPB	PMMA	4.6	0.7	*Adv. Mater.* **2019**, 31, 1807887.
15	BipyDpa	PMMA	<1	0.176	*Adv. Mater.* **2019**, 31, 1807887.
16	BipyTpa	PMMA	<1	0.028	*Adv. Mater.* **2019**, 31, 1807887.
17	PhenDpa	PMMA	5.7	0.33	*Adv. Mater.* **2019**, 31, 1807887.
18	PhenTpa	PMMA	1.2	0.68	*Adv. Mater.* **2019**, 31, 1807887.
19	TDI	PVA	37.7	0.0289	*Adv. Funct. Mater.* **2021**, 31, 2010659.
20	MeTO	PVA	24.5	0.02	*Adv. Funct. Mater.* **2021**, 31, 2010659.
21	HTO	PVA	44	0.0105	*Adv. Funct. Mater.* **2021**, 31, 2010659.
22	FTO	PVA	38	0.0174	*Adv. Funct. Mater.* **2021**, 31, 2010659.

23	CTO	PVA	39.7	0.0161	*Adv. Funct. Mater.* **2021**, 31, 2010659.
24	BrTO	PVA	26	0.0042	*Adv. Funct. Mater.* **2021**, 31, 2010659.
25	BrPmDI	PMMA	54.7	0.0014	*Angew. Chem. Int. Ed.* **2021**, 60, 12323-12327
26	IPmDI	PMMA	2.4	$6.3*10^{-6}$	*Angew. Chem. Int. Ed.* **2021**, 60, 12323-12327
27	PTzQ1	PMMA	3.8	0.0055	*Advanced Photonics Research* **2021**, 2, 2000201.
28	PTzQ2	PMMA	2.5	0.0055	*Advanced Photonics Research* **2021**, 2, 2000201.
29	(BzP)PB	PMMA	50	0.208	*Appl. Phys. Lett.* **2013** 103, 093302
30	$IBF_2dbm\text{-}OCH_3$	PMMA	9.8	0.0008	*J. Phys. Chem. A* **2017**, 121, 45, 8652–8658
31	$IBF_2dbm\text{-}F$	PMMA	8.7	0.0006	*J. Phys. Chem. A* **2017**, 121, 45, 8652–8658
32	$IBF_2dbm\text{-}CN$	PMMA	5.6	0.008	*J. Phys. Chem. A* **2017**, 121, 45, 8652–8658
33	33	Zeonex	26	0.0343	*J. Mater. Chem. C* **2017**, 5, 6269-6280.
34	34	Zeonex	14	0.0298	*J. Mater. Chem. C* **2017**, 5, 6269-6280.
35	35	Zeonex	14	0.016	*Dyes Pigment.* **2017**, 142, 315-322.
36	36	Zeonex	21	0.0064	*Dyes Pigment.* **2017**, 142, 315-322.
37	37	Zeonex	11	0.088	*Dyes Pigment.* **2017**, 142, 315-322.
38	38	Zeonex	39	0.00105	*Dyes Pigment.* **2017**, 142, 315-322.
39	39	Zeonex	2	0.0083	*Dyes Pigment.* **2017**, 142, 315-322.
40	40	Zeonex	2.9	0.0011	*Dyes Pigment.* **2017**, 142, 315-322.
41	41	Zeonex	1	0.0059	*Dyes Pigment.* **2017**, 142, 315-322.
42	BTPO-BCN	PMMA	11.6	0.822	This work
43	BTPO-BCZ	PMMA	10.6	0.73	This work
44	BTPO-TPA	PMMA	7.4	0.34	This work

Thermodynamic properties

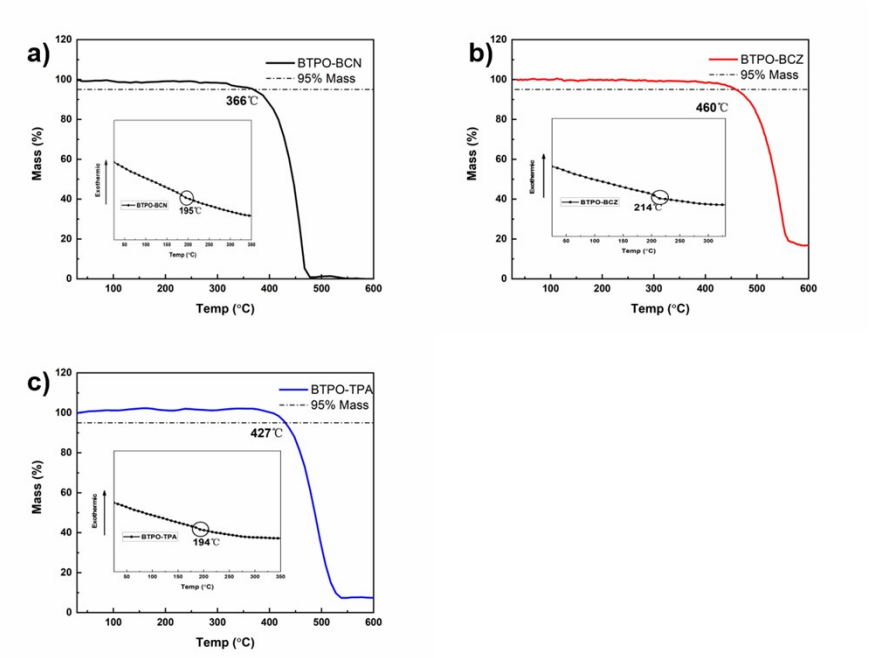

Figure S2. TG curves and DSC curves (inset) of BTPO derivates.

High performance liquid chromatography spectra

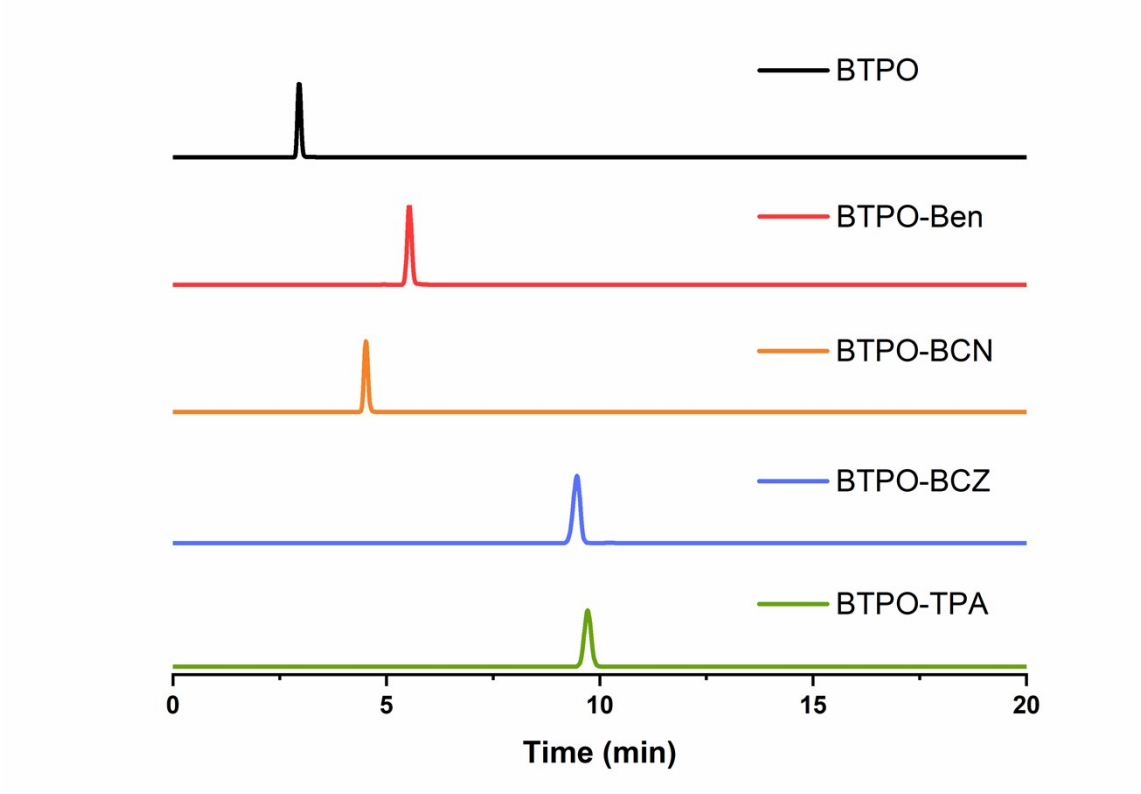

Figure S3. High performance liquid chromatography spectra of BTPO and BTPO derivative.

Photophysical properties

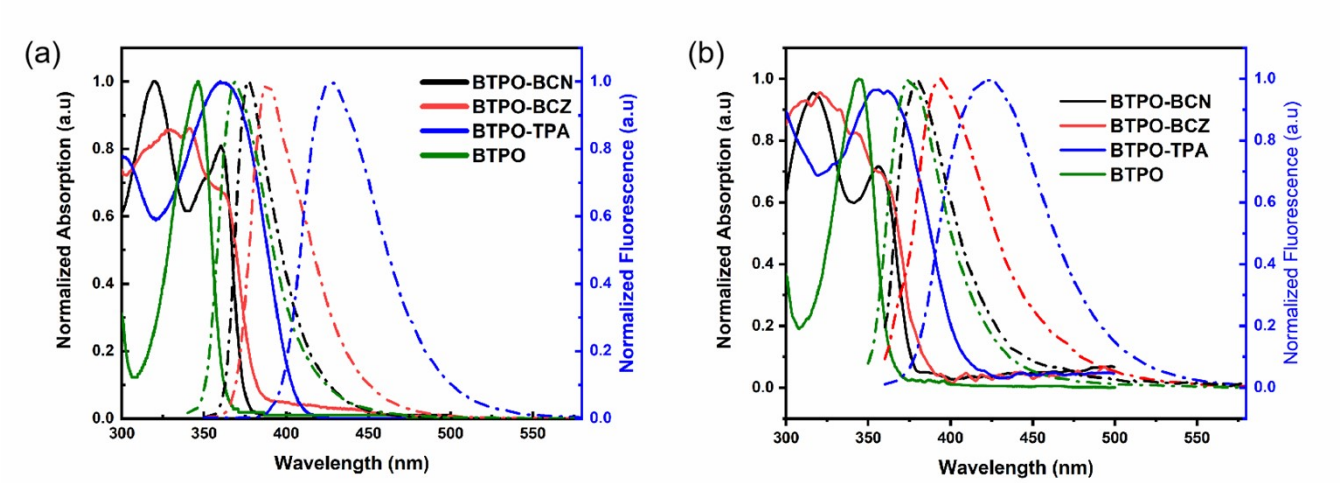

Figure S4. Normalized absorption (solid line) and fluorescence spectra (dash dot line) of BTPO and BTPO derivates measured in 10^{-5} M toluene (a) and 5wt% doped in PMMA film(b).

Table S2. Photophysical properties of BTPO and BTPO derivates in air.

Compound	10^{-5} M in toluene				5 wt% doped in PMMA film			
	λ_{abs} / nm	λ_{em} / nm	FWHM / nm	Stokes shift / nm	λ_{abs} / nm	λ_{em} / nm	FWHM / nm	Stokes shift / nm
BTPO	346	369	34	23	344	375	40	29

BTPO-BCN	360	377	28	17	356	380	39	24
BTPO-BCZ	361	388	38	27	356	393	50	37
BTPO-TPA	360	429	52	69	358	425	70	67

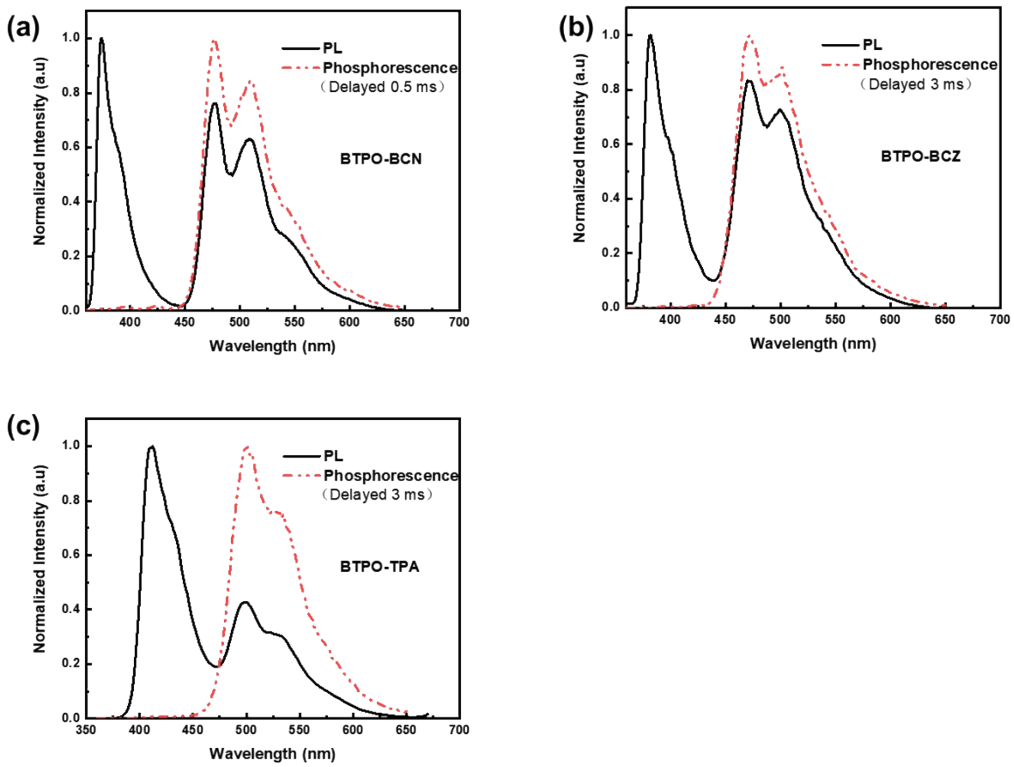

Figure S5. Steady PL and delayed PL spectra of BTPO derivatives measured in 10^{-5} M toluene at 77 K.

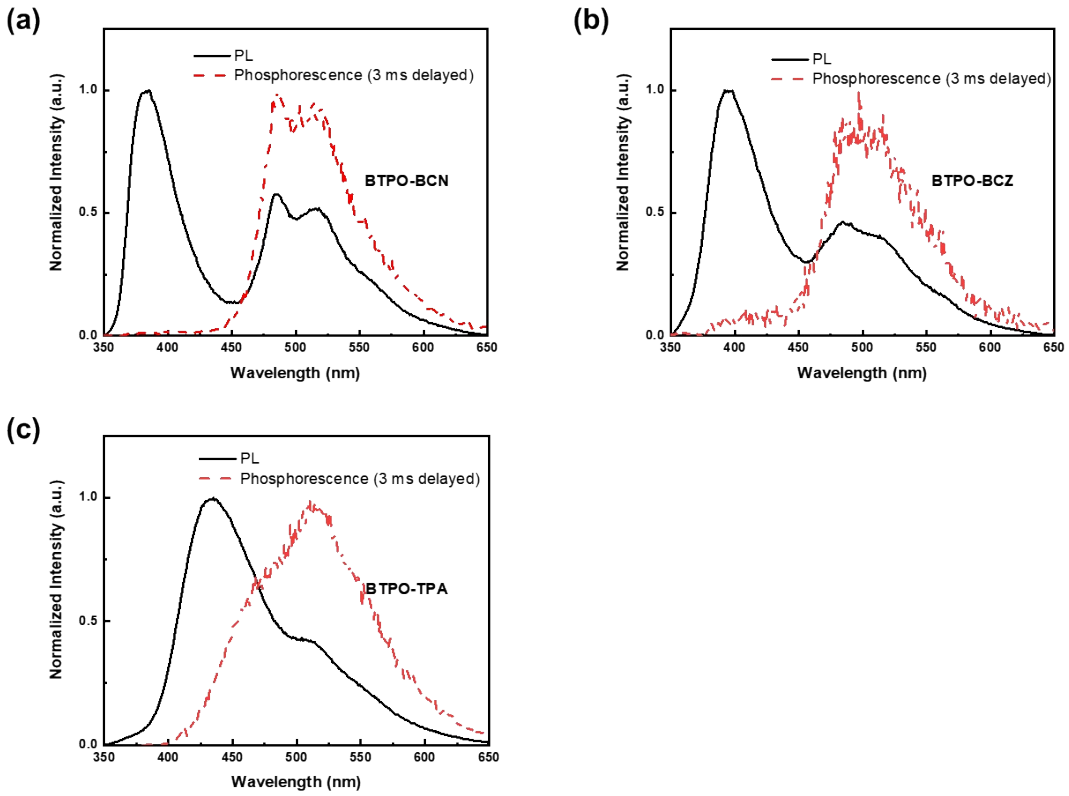

Figure S6. Steady PL and delayed PL spectra of BTPO derivatives measured in doped PMMA film at room temperature in vacuum.

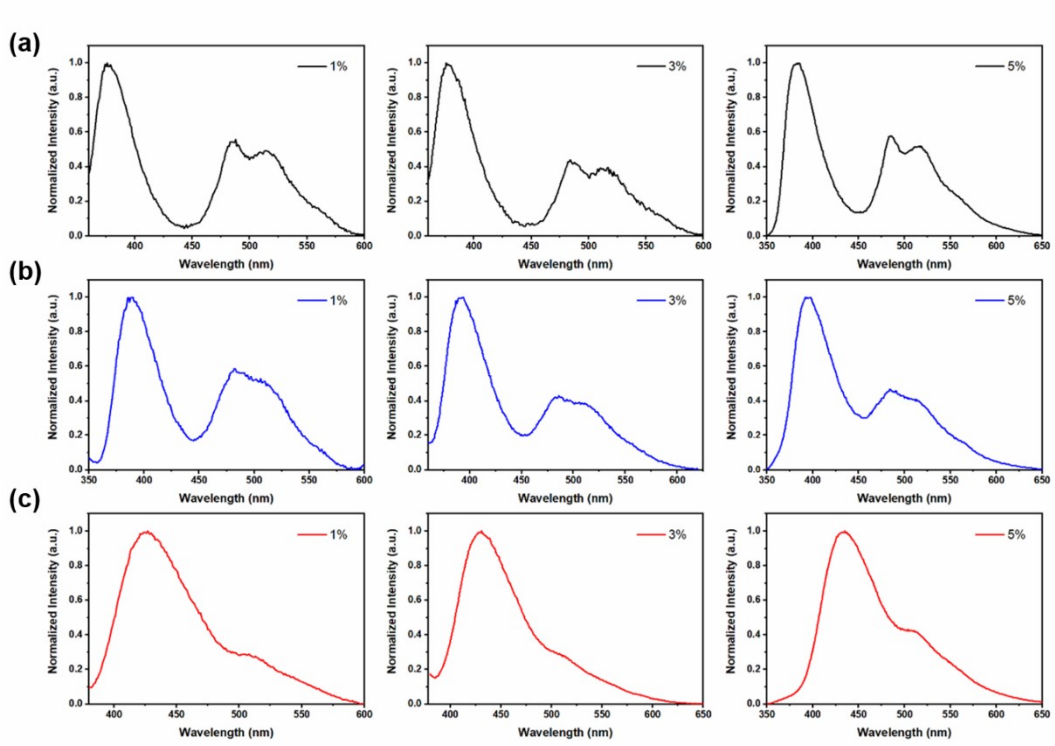

Figure S7. The steady PL spectra measurements of BTPO derivative doped in PMMA with varied concentration at room temperature: (a) BTPO-BCN; (b) BTPO-BCZ and (c) BTPO-TPA.

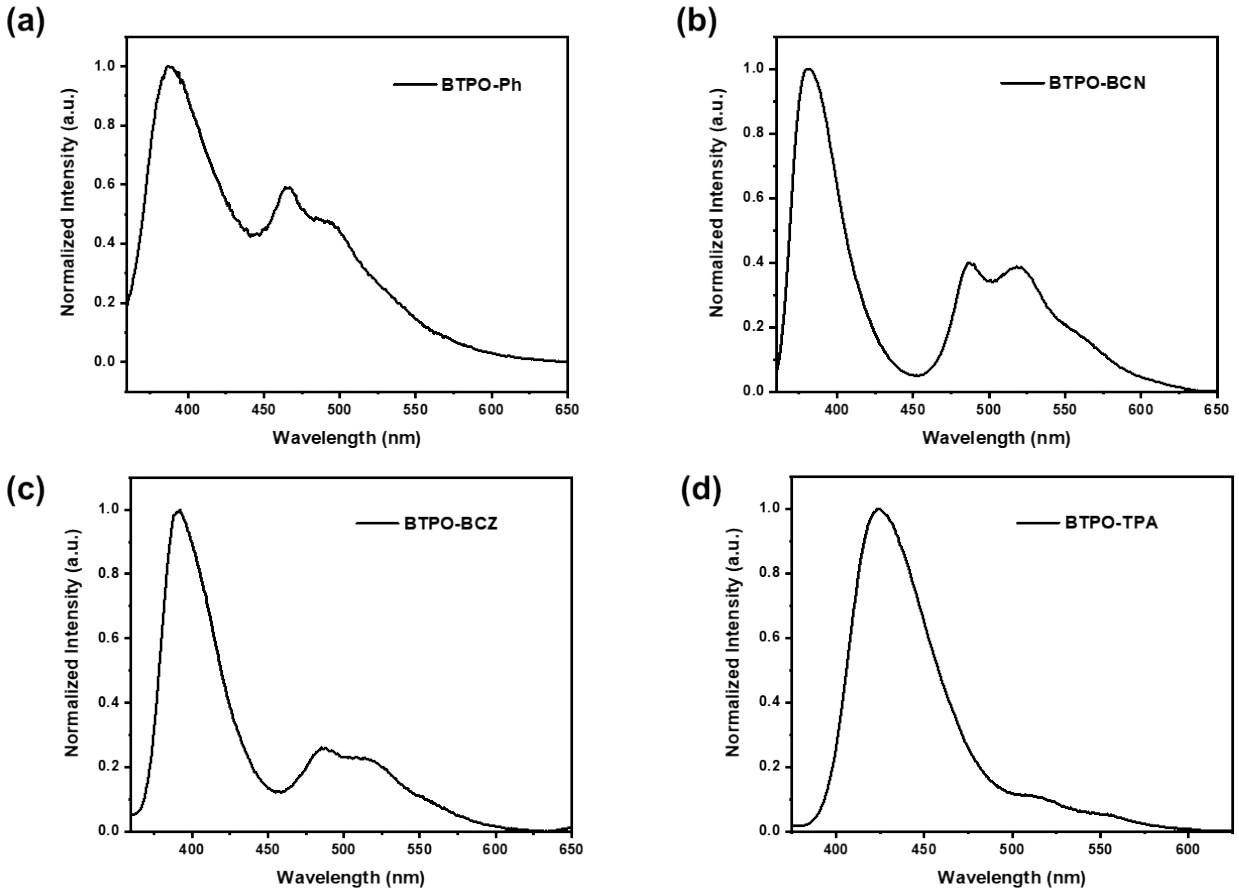

Figure S8. Steady PL spectra of BTPO derivatives measured in doped PS film at room temperature in vacuum.

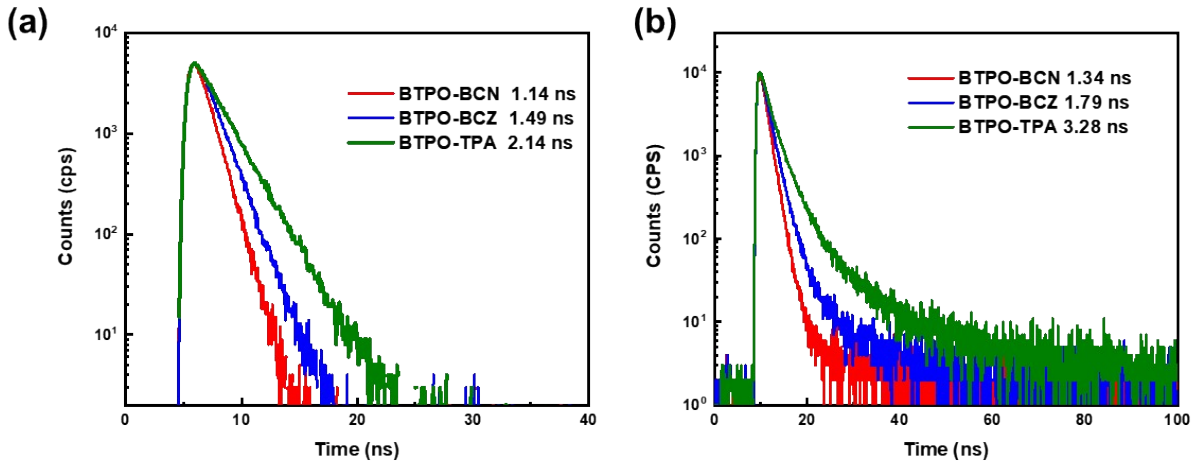

Figure S9. Transient fluorescence decay spectra of BTPO derivates measured in 10^{-5} M toluene (a) and 5wt% doped in PMMA film(b) in air.

Table S3. Photophysical properties of BTPO derivatives.

Compound	10^{-5} M in Tol measured at 77 K					5 wt% doped in PMMA measured at room-temperature in vacuum				
	λ_{fl} [nm]	S_1 [eV]	λ_{phos} [nm]	T_1 [eV]	ΔE_{ST} [eV]	λ_{fl} [nm]	S_1 [eV]	λ_{phos} [nm]	T_1 [eV]	ΔE_{ST} [eV]
BTPO-BCN	373	3.32	477	2.60	0.72	382	3.25	486	2.55	0.70

BTPO-BCZ	381	3.25	472	2.63	0.62	394	3.15	485	2.56	0.59
BTPO-TPA	412	3.00	501	2.48	0.52	432	2.87	510	2.43	0.44

Table S4. Dynamic photophysical parameters of BTPO derivatives in doped PMMA film at toom temperature.

compound	Fluorescence					Phosphorescence			
	T_{fluo}/ns	φ_{fluo}/%	$k_{r(fluo)}/10^7\ s^{-1}$	$k_{nr(fluo)}/10^7\ s^{-1}$	$k_{(ISC)}/10^7\ s^{-1}$	T_{phos}/ms	φ_{phos}/%	$k_{r(phos)}/s^{-1}$	$k_{nr(phos)}/s^{-1}$
BTPO-BCN	1.34	14.2	10.60	57.01	7.01	822	11.6	0.114	1.10
BTPO-BCZ	1.79	21.3	11.90	38.04	5.92	730	10.6	0.145	1.22
BTPO-TPA	3.28	29.4	8.96	19.27	2.68	340	7.4	0.218	2.72

$k_{r(fluo)} = \varphi_{fluo}/T_{fluo}$; $k_{nr(fluo)} = (1-\varphi_{fluo}-\varphi_{phos})/T_{fluo}$; $k_{ISC} = \varphi_{phos}/T_{fluo}$; $k_{r(phos)} = \varphi_{phos}/T_{phos}$; $k_{nr(phos)} = (1-\varphi_{phos})/T_{phos}$;

The dynamic photophysical parameters of BTPO derivatives were calculated according to the previous reported methods[3, 4] based on the quantum yields and lifetime of fluorescence and phosphorescence. Due to multiple heteroatoms (S, O, N) on such rigid interlocked scaffold along with excited states modulation, BTPO derivatives exhibit efficient ultralong room-temperature phosphorescence. Especially, the introduction of the sulfone group on the conjugated skeleton weakens the delocalization of electron pairs on the oxygen to π-conjugated skeleton, reducing the contribution of (n, π*) transition to triplet excited state. Combined with the further modification of the periphery groups, the triplet states of BTPO derivatives tend to present a much purer configuration of (π, π*), which conduce to long phosphorescence lifetimes of over 0.3 s and lower phosphorescent radiative decay rates for BTPO derivatives[3, 4].

To be noted, an upward trend of phosphorescent radiative decay rate constants was observed from BTPO-BCN to BTPO-BCZ and further to BTPO-TPA, which is probably attributed to the increased proportion of (n, π*) transition caused by the lone electron pair of nitrogen atom in triplet excited state. As for the phosphorescent non-radiative decay rate constants, an ascending tendency as well was found from BTPO-BCN to BTPO-TPA. This may be due to the enhanced charge transfer characteristics for T_1 state along with more flexible substituents that might lead to greater vibrations in triplet configuration and cause more energy dissipation.

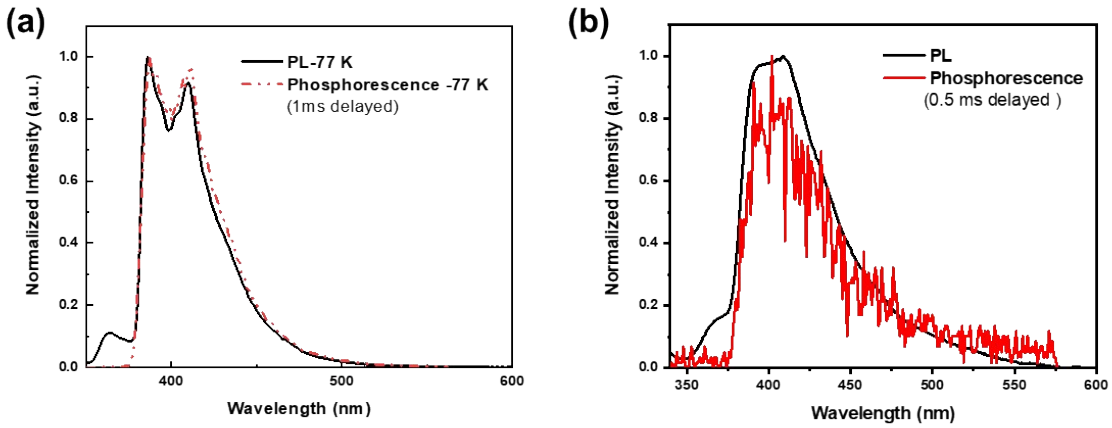

Figure S10. Steady PL and delayed PL spectra of BTPO measured in 10^{-5} M toluene (a) and 5wt% doped in PMMA film(b) at low temperature.

Table S5. Photophysical properties of BTPO at low temperature.

Compound	10^{-5} M in Tol measured at 77 K					5 wt% doped in PMMA measured at 100 K in vacuum				
	λ_{fl} [nm]	S_1 [eV]	λ_{phos} [nm]	T_1 [eV]	$E_{\Delta ST}$ [eV]	λ_{fl} [nm]	S_1 [eV]	λ_{phos} [nm]	T_1 [eV]	$E_{\Delta ST}$ [eV]
BTPO	363	3.41	387	3.20	0.21	375	3.31	394	3.15	0.16

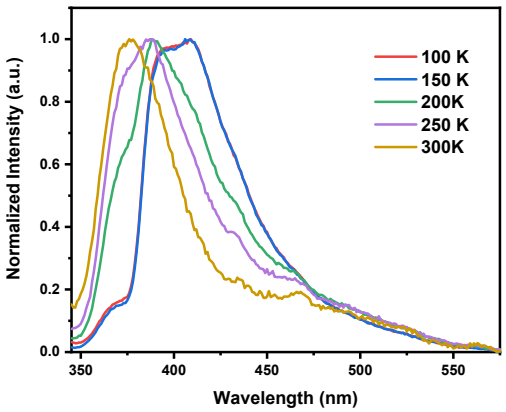

Figure S11. Steady PL spectra of BTPO 5wt% doped in PMMA film measured at varied temperature in vacuum.

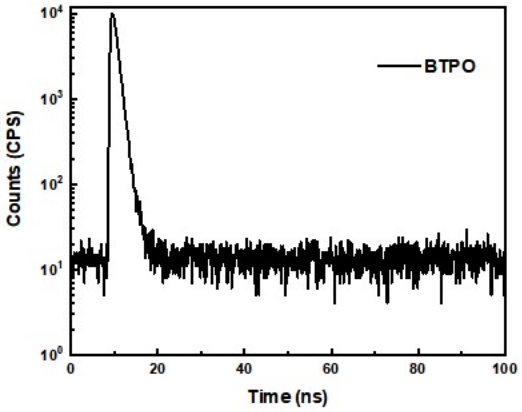

Figure S12. Fluorescence decay spectra of BTPO measured at 375nm in doped PMMA film in time range of 100 ns at 300 K in vacuum, .

Table S6. Lifetime of 5wt% BTPO doped in PMMA film in vacuum.

Compound	$\tau_{promote}$ [ns]	$\tau_{delayed}$ [μs]
BTPO	1.04	τ_{avg} = 41.04, τ_1 = 6.29, τ_2 = 103.66

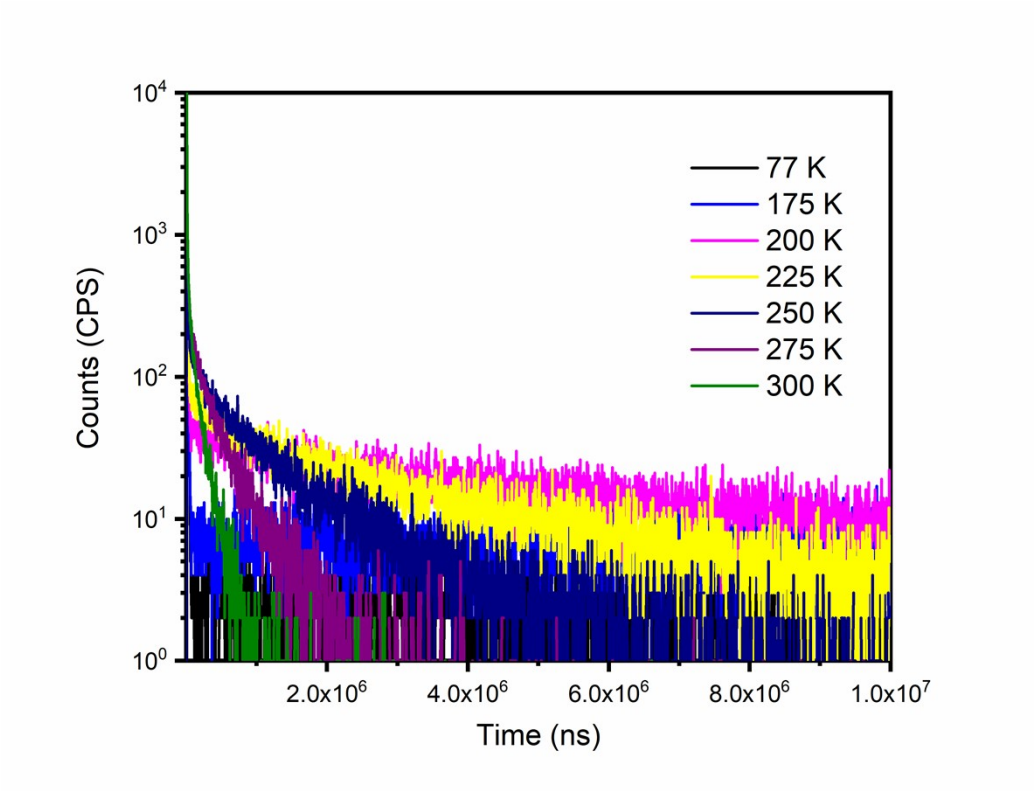

Figure S13. Fluorescence decay spectra of BTPO measured at 370nm in 5 wt% doped PMMA film in time range of 10 ms at varied temperature in vacuum

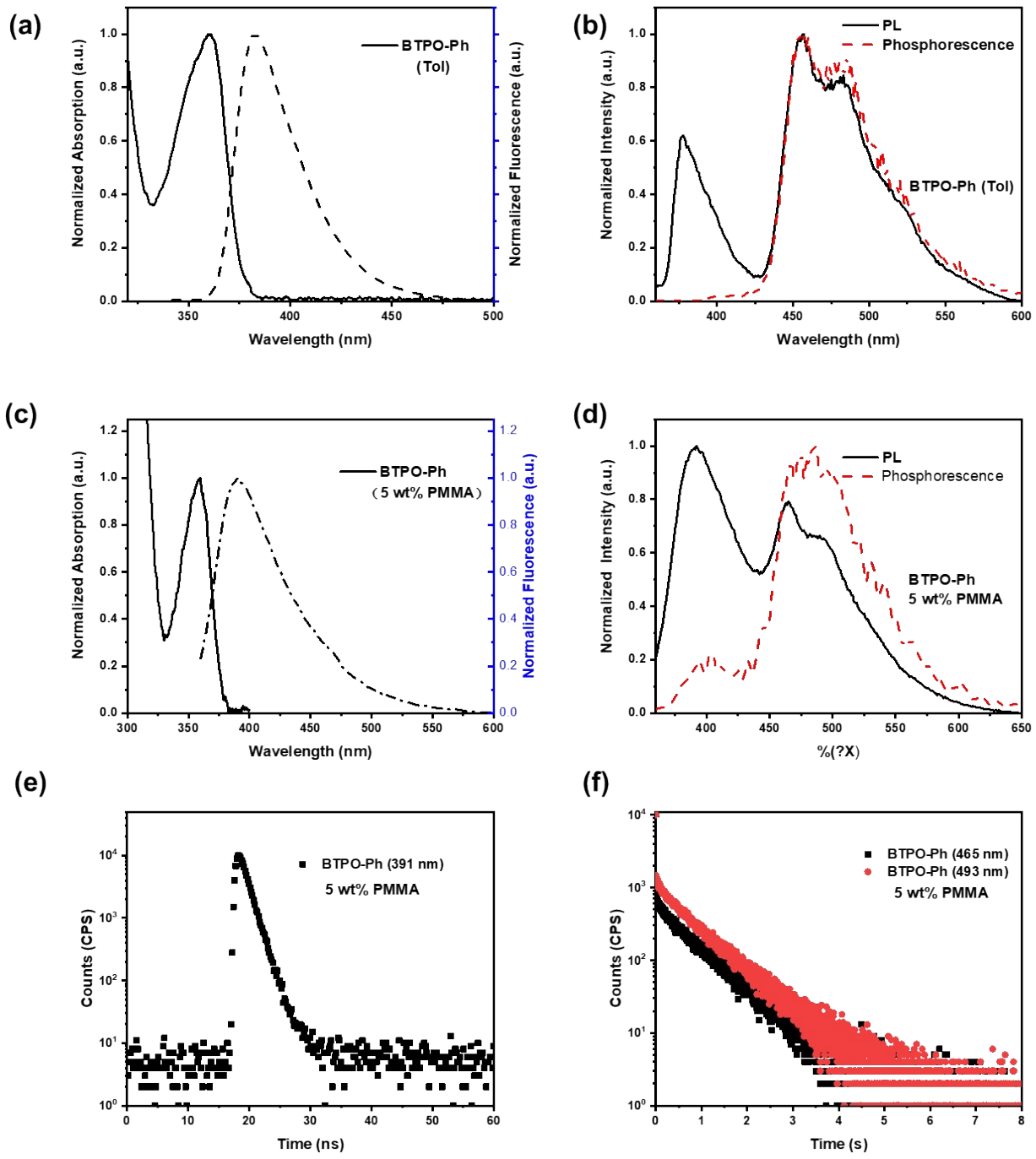

Figure S14. Normalized absorption and fluorescence spectra of BTPO-Ph measured in 10^{-5} M toluene (a) and 5wt% doped in PMMA film(c); Steady PL and delayed PL spectra of BTPO-Ph measured in 10^{-5} M toluene at 77 K (b) and in doped PMMA film at room temperature in vacuum (d); Fluorescence (e) and phosphorescence (f) decay spectra of BTPO-Ph measured at 369nm in doped PMMA film at 300 K.

Table S7. Photophysical properties of BTPO derivatives.

Compound	10^{-5} M in Tol measured at RT		10^{-5} M in Tol measured at 77 K		5 wt% doped in PMMA measured at room-temperature in vacuum				
	λ_{abs} [nm]	λ_{fl} [nm]	λ_{fl} [nm]	λ_{phos} [nm]	λ_{abs} [nm]	λ_{fl} [nm]	λ_{phos} [nm]	T_{fluo} [ns]	T_{phos} [ms]
BTPO-Ph	360	382	377	456	359	391	465	1.27	658

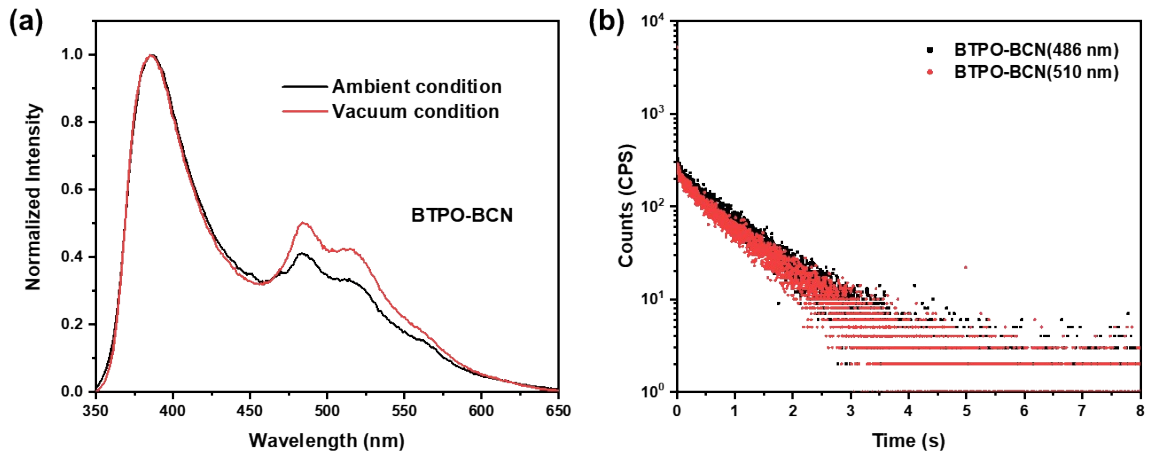

Figure S15. (a) Steady PL spectra of BTPO-BCN measured in doped PMMA film coated by PVA layer at room temperature under ambient condition an in vacuum. (b) PL decay profile of BTPO-BCN measured in doped PMMA film coated by PVA layer at room temperature in vacuum.

Table S8. Dynamic photophysical parameters of BTPO derivatives in doped PMMA film coated by PVA at toom temperature.

compound	Fluorescence					Phosphorescence			
	T_{fluo}/ns	φ_{fluo}/%	$k_{r(fluo)}/10^7\ s^{-1}$	$k_{nr(fluo)}/10^7\ s^{-1}$	$k_{(ISC)}/10^7\ s^{-1}$	T_{phos}/ms	φ_{phos}/%	$k_{r(phos)}/s^{-1}$	$k_{nr(phos)}/s^{-1}$
BTPO-BCN	1.28	14.50	11.33	60.07	6.72	743	8.6	0.116	1.23

$k_{r(fluo)} = \varphi_{fluo}/T_{fluo}$; $k_{nr(fluo)} = (1-\varphi_{fluo}\cdot\varphi_{phos})/T_{fluo}$; $k_{ISC} = \varphi_{phos}/T_{fluo}$; $k_{r(phos)} = \varphi_{phos}/T_{phos}$; $k_{nr(phos)} = (1-\varphi_{phos})/T_{phos}$;

Theoretical Calculation

The excitation energy and natural transition orbitals (NTO) were evaluated at TD-M062X/6-31G (d, p) level by Gaussian 09 program[5]. At the same level, the oscillator strengthens *f* and spin-orbit coupling (SOC) were evaluated using BDF program[6].

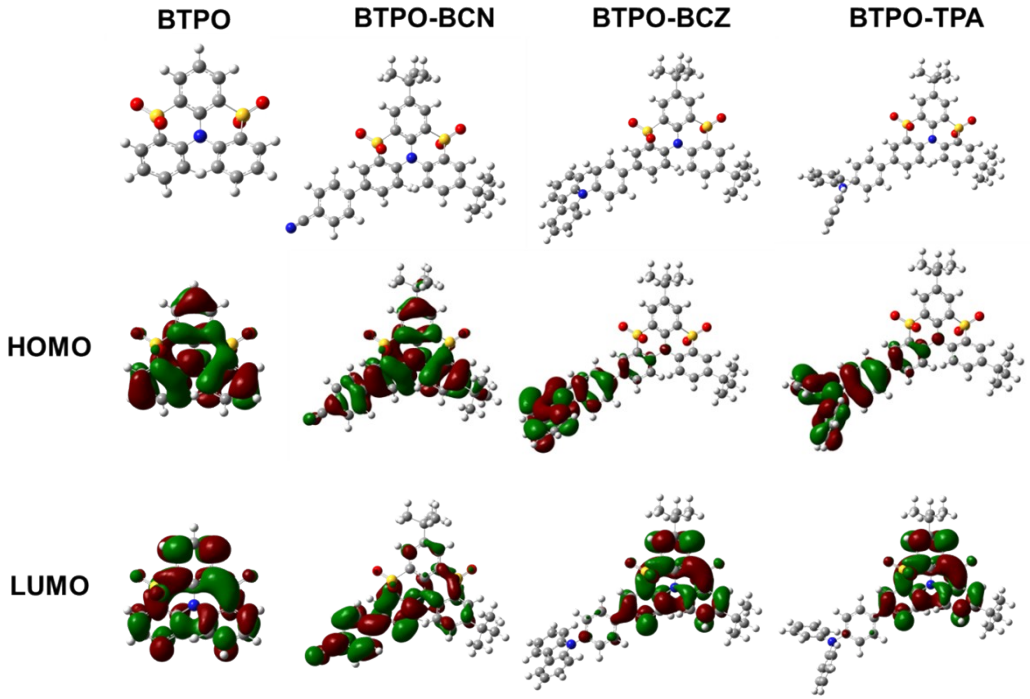

Figure S16. Calculated molecular structure and frontier orbitals (FMOs) of BTPO and BTPO derivatives.

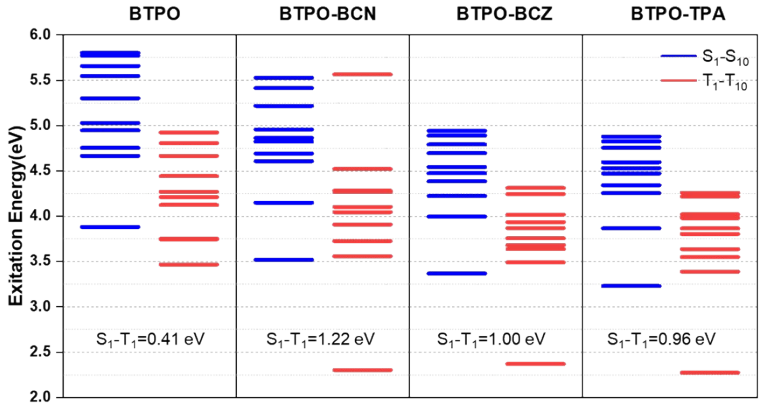

Figure S17. Calculated energy level diagrams of BTPO and BTPO derivatives.

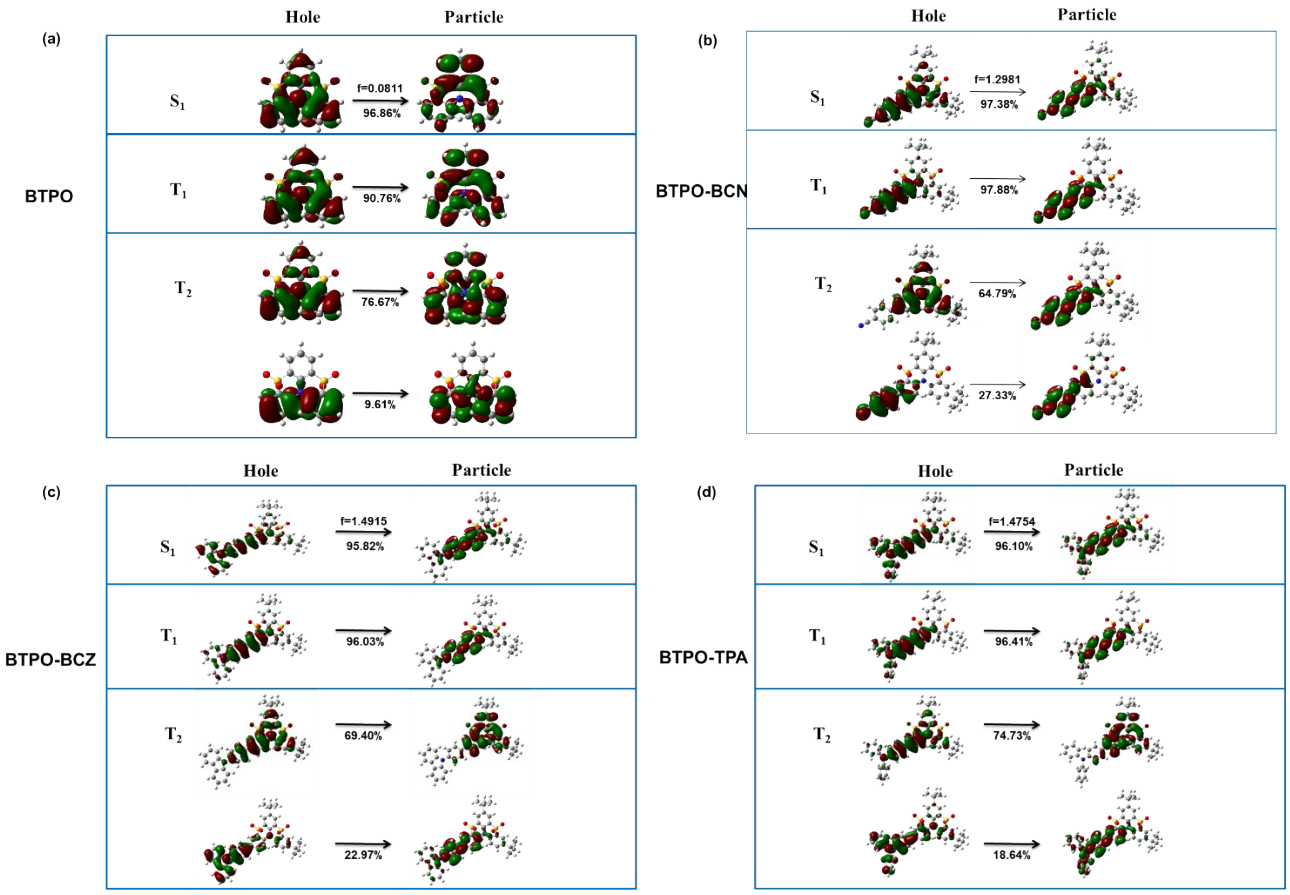

Figure S18. Natural transition orbitals of BTPO and BTPO derivatives.

Table S9. Spin-orbit coupling (SOC) constants of BTPO and BTPO derivatives.

Compound	$\langle S_0\|\hat{H}_{SO}\|T_1\rangle$	$\langle S_1\|\hat{H}_{SO}\|T_1\rangle$	$\langle S_1\|\hat{H}_{SO}\|T_2\rangle$	$\langle S_1\|\hat{H}_{SO}\|T_3\rangle$	$\langle S_1\|\hat{H}_{SO}\|T_4\rangle$
BTPO	2.049	0.008	1.155	1.358	3.085
BTPO-BCN	1.013	0.303	0.300	0.399	0.565
BTPO-BCZ	1.000	0.425	0.282	0.319	0.777
BTPO-TPA	1.035	0.349	0.148	0.311	0.196

Solvatochromic effect

The properties of ground state (S_0) and the lowest singlet excited state (S_1) can be better understood through solvatochromic experiment. We use the Lippert-Mataga equation to explore the influence of solvent environment on the optical property of our materails, the model can describe the interaction between the solvent and the dipole moment of solute:

$$hc(\nu_a - \nu_f) = hc(\nu_a^0 - \nu_f^0) - \frac{2(\mu_e - \mu_g)^2}{a^3} f(\varepsilon, n$$

where *f* is the orientational polarizability of the solvent, $\nu_a^0 - \nu_f^0$ corresponds to the Stokes shifts when *f* is zero, μ_e is the excited state dipole moment, μ_g is the ground-state dipole moment; *a* is the solvent cavity (Onsager) radius, derived from the Avogadro number (*N*), molecular weight (M), and density (d = 1.0 g cm^{-3}); ε and *n* are the solvent dielectric and the solvent refractive index, respectively; *f*(ε, *n*) and *a* can be calculated respectively as follows:

$$f(\varepsilon, n) = \frac{\varepsilon - 1}{2\varepsilon + 1} - \frac{n^2 - 1}{2n^2 + 1}$$

$$a = \left(\frac{3M}{4N\pi d}\right)^{1/3}$$

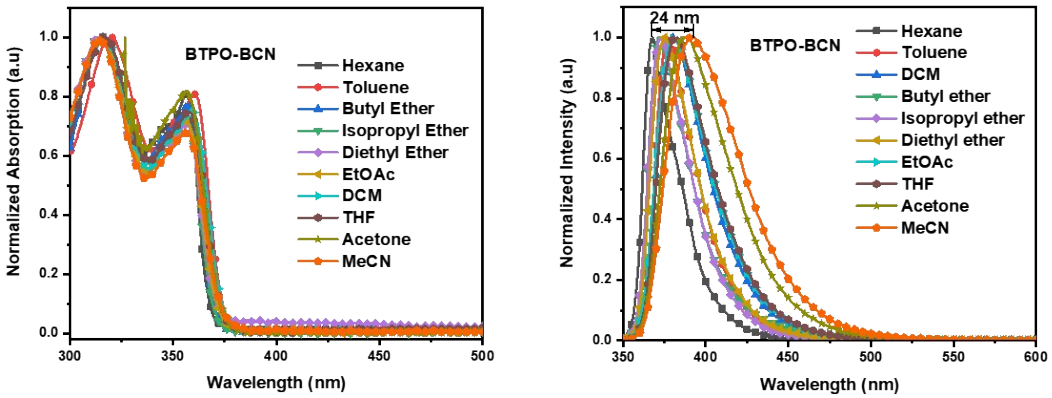

Figure S19. Normalized absorption (right) and fluorescence (left) spectra of BTPO-BCN measured in different solvents.

Table S10. Detailed absorption and emission peak positions of BTPO-BCN in different solvents.

Solvent	*n*	ε	*f*(ε, *n*)	λ_{abs} [nm]	λ_{em} [nm]	FWHM [nm]	Stokes shift [nm]	ν_a-ν_f [cm^{-1}]
Hexane	1.375	1.9	0.0012	356	368	24	12	916
Toluene	1.497	2.38	0.014	360	377	28	17	1253
Butyl ether	1.399	3.08	0.096	357	372	28	15	1129
Isopropyl ether	1.368	3.88	0.145	356	372	28	16	1208
Diethyl ether	1.352	4.34	0.167	356	375	31	19	1423
EtOAc	1.372	6.02	0.2	357	381	37	24	1764
THF	1.407	7.58	0.21	358	382	37	24	1755
DCM	1.424	8.93	0.217	359	380	34	21	1539
Acetone	1.359	20.7	0.284	356	387	47	31	2250
MeCN	1.344	37.5	0.305	360	392	52	32	2268

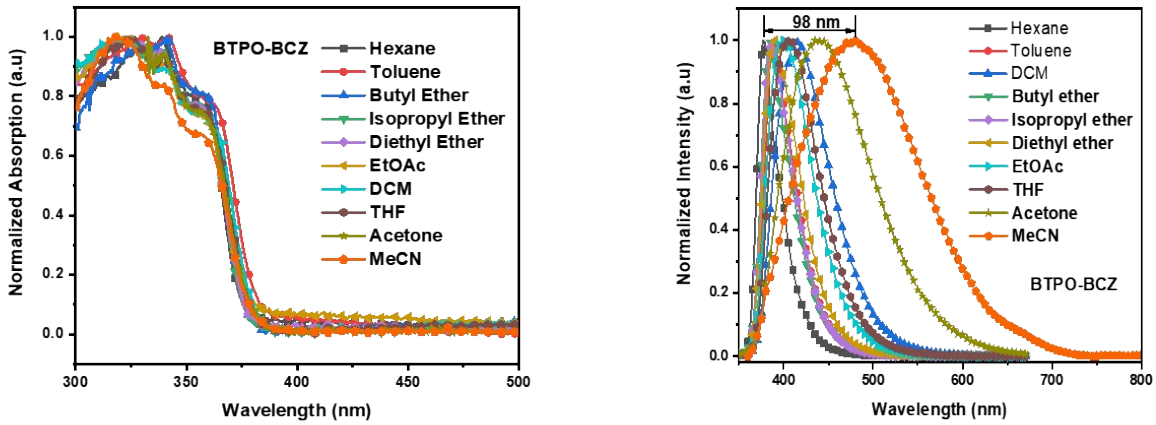

Figure S20. Normalized absorption (right) and fluorescence (left) spectra of BTPO-BCZ measured in different solvents.

Table S11. Detailed absorption and emission peak positions of BTPO-BCZ in different solvents.

Solvent	*n*	*ε*	*f*(*ε*, *n*)	λ_{abs} [nm]	λ_{em} [nm]	FWHM [nm]	Stokes shift [nm]	ν_a-ν_f [cm^{-1}]
Hexane	1.375	1.9	0.0012	359	377	29	18	1330
Toluene	1.497	2.38	0.014	361	388	38	27	1928
Butyl ether	1.399	3.08	0.096	359	384	37	25	1813
Isopropyl ether	1.368	3.88	0.145	357	386	40	29	2104
Diethyl ether	1.352	4.34	0.167	357	390	47	33	2370
EtOAc	1.372	6.02	0.2	358	400	58	42	2933
THF	1.407	7.58	0.21	358	407	63	49	3363
DCM	1.424	8.93	0.217	358	417	71	59	3952
Acetone	1.359	20.7	0.284	358	436	115	78	4997
MeCN	1.344	37.5	0.305	357	479	158	122	7134

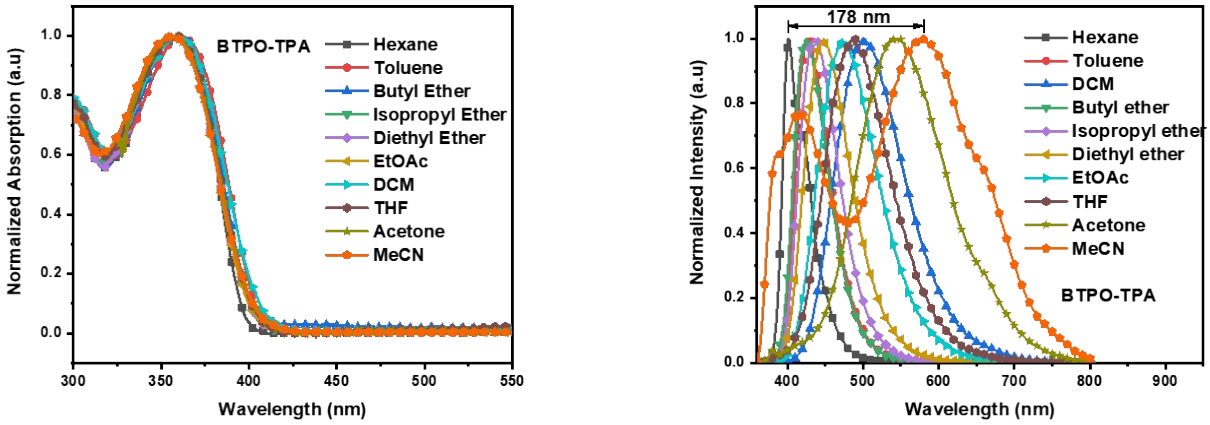

Figure S21. Normalized absorption (right) and fluorescence (left) spectra of BTPO-TPA measured in different solvents.

Table S12. Detailed absorption and emission peak positions of BTPO-TPA in different solvents.

Solvent	*n*	*ε*	*f*(*ε*, *n*)	λ_{abs} [nm]	λ_{em} [nm]	FWHM [nm]	Stokes shift [nm]	ν_a-ν_f [cm^{-1}]
Hexane	1.375	1.9	0.0012	359	401	38	42	2917
Toluene	1.497	2.38	0.014	360	429	52	69	4468
Butyl ether	1.399	3.08	0.096	359	425	53	66	4326
Isopropyl ether	1.368	3.88	0.145	358	436	61	78	4997
Diethyl ether	1.352	4.34	0.167	359	448	70	90	5534
EtOAc	1.372	6.02	0.2	358	472	91	114	6747

THF	1.407	7.58	0.21	358	487	97	129	7399
DCM	1.424	8.93	0.217	358	503	105	145	8052
Acetone	1.359	20.7	0.284	357	544	132	187	9629
MeCN	1.344	37.5	0.305	355	579	299	224	10898

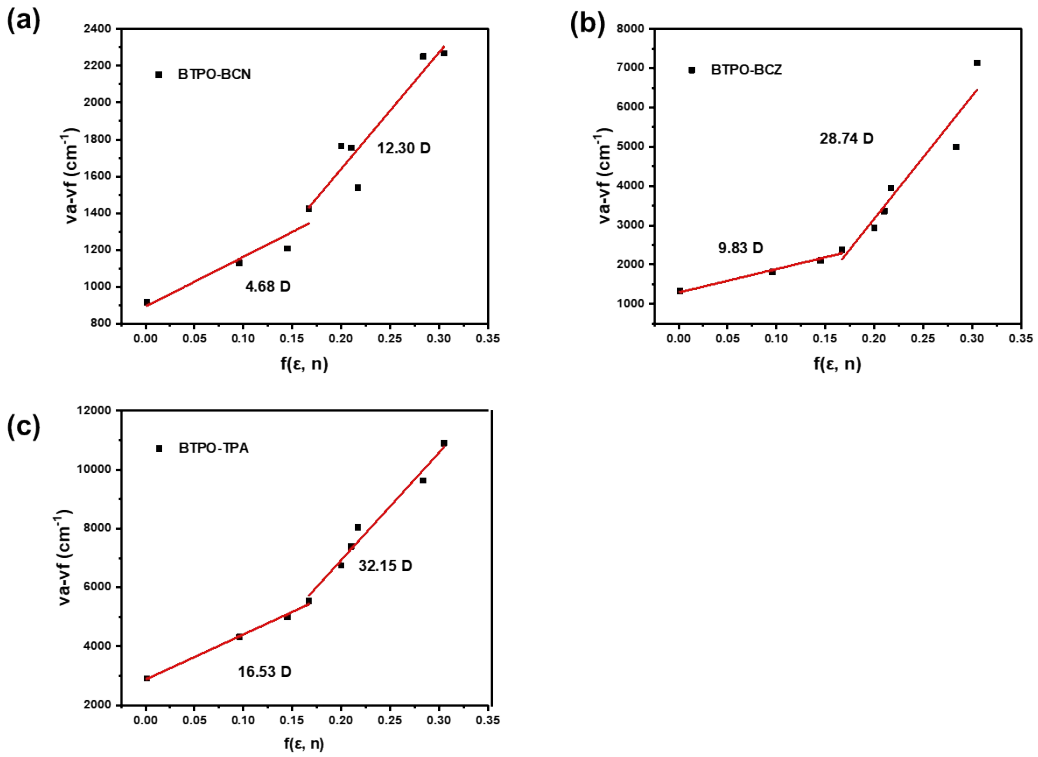

Figure S22. Linear correlation of orientational polarization (*f*) of solvent media with the Stokes shift (va-vf; a: absorbed light; f: fluorescence) for BTPO derivatives.

Phosphorescence graph

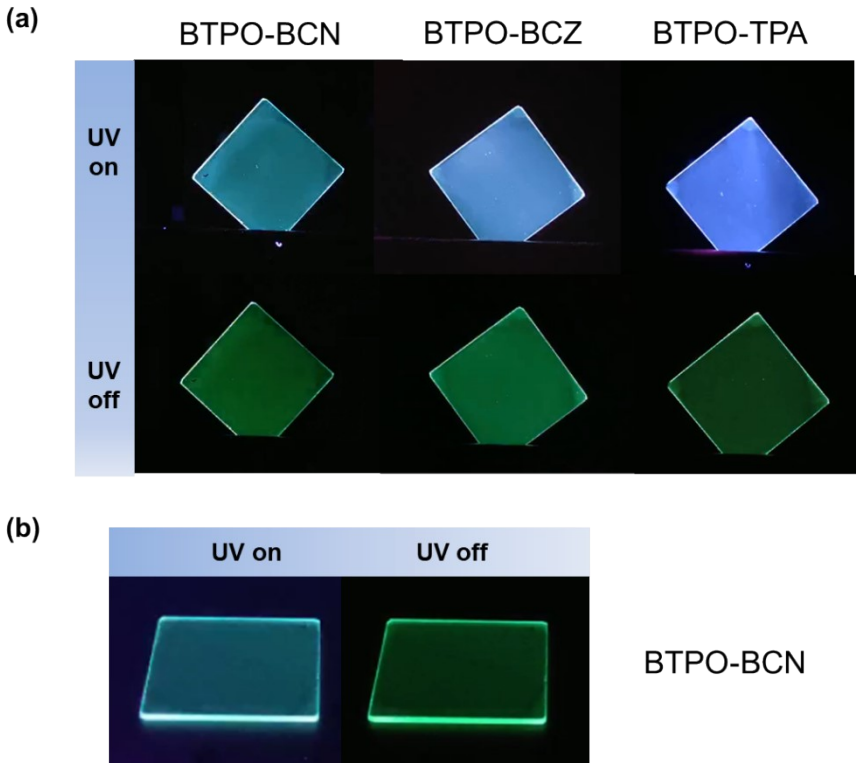

Figure S23. photographs of (a) BTPO-derivates in PMMA film in vacuum and (b) BTPO-BCN in PMMA film covered by PVA in air under UV lamp and after the removal of UV source.

Supplementary Video

Video 1. When excited by a 365 nm UV lamp, 5wt% BTPO-BCN doped in PMMA film exhibited bluish-green luminescence. After removal of the light source, the emission color turned green, easily observed by the naked eyes.
Video 2. When excited by a 365 nm UV-lamp, 5wt% BTPO-BCZ doped in PMMA film exhibited blue luminescence. After the removal of the emission color turned green, easily observed by the naked eyes.
Video 3. When excited by a 365 nm UV-lamp, 5wt% BTPO-TPA doped in PMMA film exhibited blue luminescence. After the removal of the emission color turned green, easily observed for several seconds by the naked eyes.
Video 4. When excited by a 365 nm UV lamp, 5wt% BTPO-BCN doped in PMMA film covered by a PVA layer exhibited bluish-green luminescence under ambient condition. After removal of the light source, the emission color turned green, easily observed by the naked eyes.
Video 5. When excited by a 365 nm UV lamp, the pattern exhibited cyan-blue luminescence. After removal of the light source, the emission color turned green, easily observed by the naked eyes.
Video 6. When excited by a 365 nm UV lamp, the pattern of SCUT exhibited cyan-blue luminescence. After removal of the light source, the emission color turned green, easily observed by the naked eyes.

Electrochemical properties

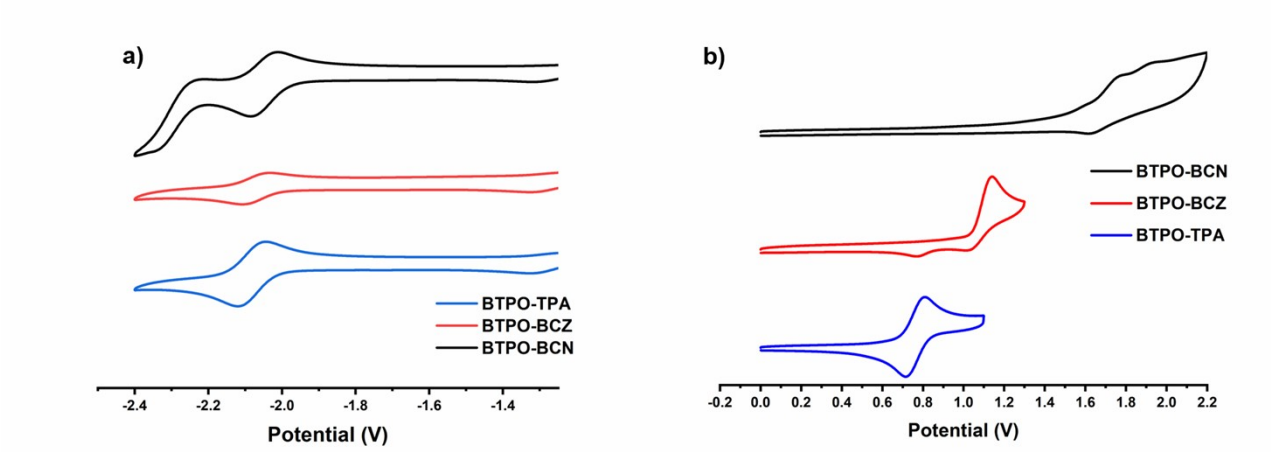

Figure S24. Cyclic voltammetry spectra of BTPO derivates measured in DMF (a) and DCM (b).

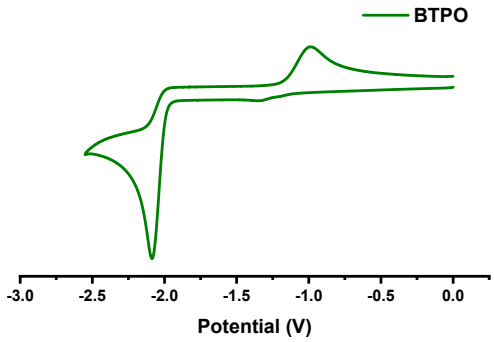

Figure S25. Cyclic voltammetry spectra of BTPO measured in DMF.

Table S13.Electrochemical properties of BTPO and BTPO derivates.

Compound	E_{LUMO} / eV [a]	E_{HOMO} / eV [b]	E_g / eV [c]
BTPO-BCN	-2.76	-6.03	3.27
BTPO-BCZ	-2.73	-5.62	2.89
BTPO-TPA	-2.73	-5.26	2.53
BTPO	-2.77	-6.17[e]	3.40[f]

[a] Estimated from the onset potential of the first reduction wave and calculated according to $E_{LUMO} = -(4.8 + E_{onset}^{re})$ eV. [b] Estimated from the onset potential of the first oxidation wave and calculated according to $E_{HOMO} = -(4.8 + E_{onset}^{ox})$ eV. [c] Calculated according to $E_g = (E_{LUMO} - E_{HOMO})$ eV. [e] $E_{HOMO} = E_{LUMO} - E_g$. [f] $Eg = 1240 / \lambda_{onset}$.

The electrochemical properties of BTPO and BTPO derivatives were investigated by cyclic voltammetry (CV) measurement. Observed in Figure S24a and S25, BTPO, BTPO-BCZ and BTPO-TPA exhibited one well-defined reversible reduction peak, while BTPO-BCN shows two reversible reduction peaks as a result of the introduction of the withdrawing functional group of benzonitrile. The LUMO levels of all the compounds estimated from the onset potential of the first reduction wave are -2.77 eV for BTPO, -2.76 eV for BTPO-BCN, -2.73 eV for BTPO-BCZ and -2.73 eV for BTPO-TPA, respectively. It indicated minor changes occurred on the distribution of LUMOs that remained mainly at the BTPO core, confirmed by the calculation results of the frontier orbitals. With the increased electron-donating character of substituents from BCN to BCZ, and further to TPA, the HOMO energy levels were uplifted to -6.03 eV for BTPO-BCN, -5.62 eV for BTPO-BCZ and -5.26 eV for BTPO-TPA, as compared with -6.17 eV for BTPO. Correspondingly, the

distribution of HOMOs for BTPO derivatives delocalized to the periphery groups instead of the BTPO core. The above results lead to narrower bandgaps for BTPO derivatives.

X-ray Crystallographic Analysis

Crystallographic data have been deposited with the Cambridge Crystallographic Data Centre as supplementary publication. The single crystal X-ray crystallographic data were summarized in Table S13.

Table S14. Single-crystal XRD data

Compound	BTPO-BCN
CCDC number	2079614
Empirical formula	C33H30N2O4S2
Formula weight	582.71
Crystal system	Monoclinic
Space group	C1 2/c 1
a (Å)	27.3326(6)
b (Å)	13.6010(4)
c (Å)	16.1847(3)
α (°)	90
β (°)	93.524(2)
γ (°)	90
Volume ($Å^3$)	6005.3
Density (mg/m^3)	1.289
Crystal size (mm^3)	0.1×0.08×0.06
Z	8
Data/restraints/parameters	5294/0/376
Goodness-of-fit	1.028
Final R [I>2sigma(I)]	R1=0.0454, wR2=0.1130
R indices (all data)	R1=0.0596, wR2=0.1198

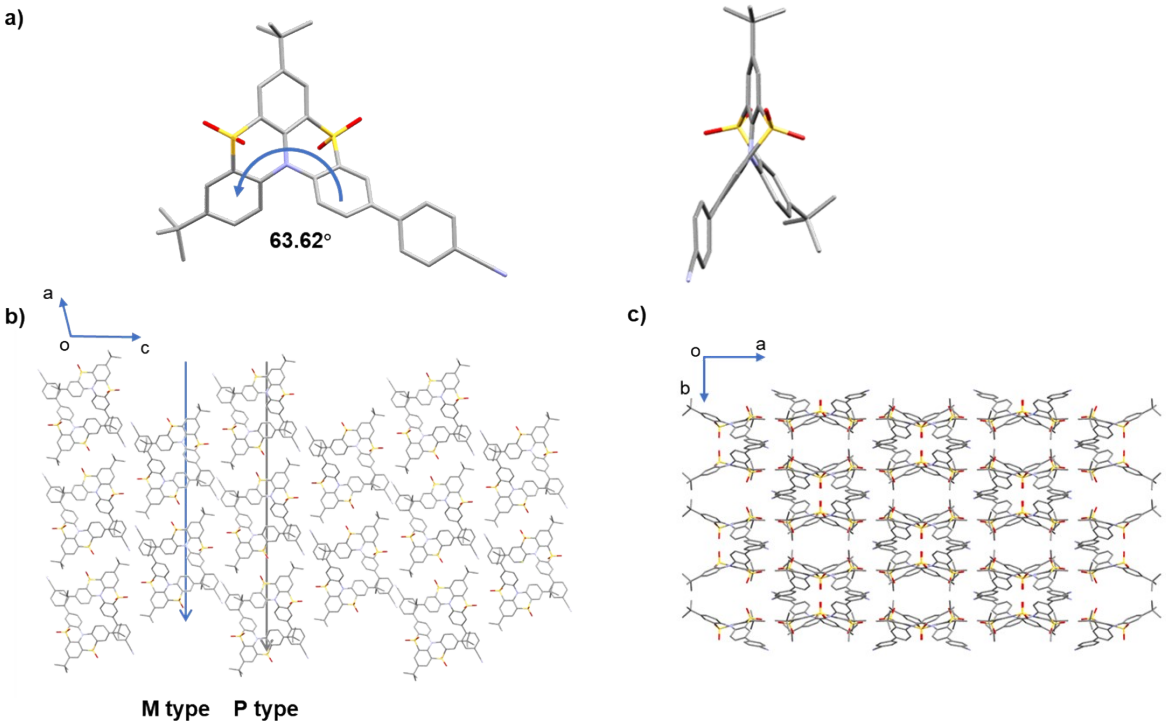

Figure S26. Crystal structure and packing arrangement of BTPO-BCN.

References

[1] S. Menichetti, C. Faggi, M. Onori, S. Piantini, M. Ferreira, S. Rocchi, M. Lupi, I. Marin, M. Maggini, C. Viglianisi, *Eur. J. Org. Chem.* **2019**, *2019*, 168-175.

[2] M. Kuratsu, M. Kozaki, K. Okada, *Chem. Lett.* **2004**, *33*, 1174-1175.

[3] Z. Yang, C. Xu, W. Li, Z. Mao, X. Ge, Q. Huang, H. Deng, J. Zhao, F. L. Gu, Y. Zhang, Z. Chi, *Angew. Chem. Int. Ed.* **2020**, 59, 17451-17455.

[4] S. Tian, H. Ma, X. Wang, A. Lv, H. Shi, Y. Geng, J. Li, F. Liang, Z. M. Su, Z. An, W. Huang, *Angew. Chem. Int. Ed.* **2019**, 58, 6645-6649.

[5] M. J. Frisch, G. W. Trucks, H. B. Schlegel, G. E. Scuseria, M. A. Robb, J. R. Cheeseman, G. Scalmani, V. Barone, B. Mennucci, G. A. Petersson, Others, *Gaussian Inc. Wallingford CT* **2009**, *27*, 34.

[6] W. Liu, F. Wang, D. Dai, L. Li, M. Dolg, The Beijing Four-Component Density Functional Program Package (BDF) And Its Application to EuO, EuS, YbO and YbS. *Theor. Chem. Acc.* **1997**, *96*, 75-83.

NMR Spectra

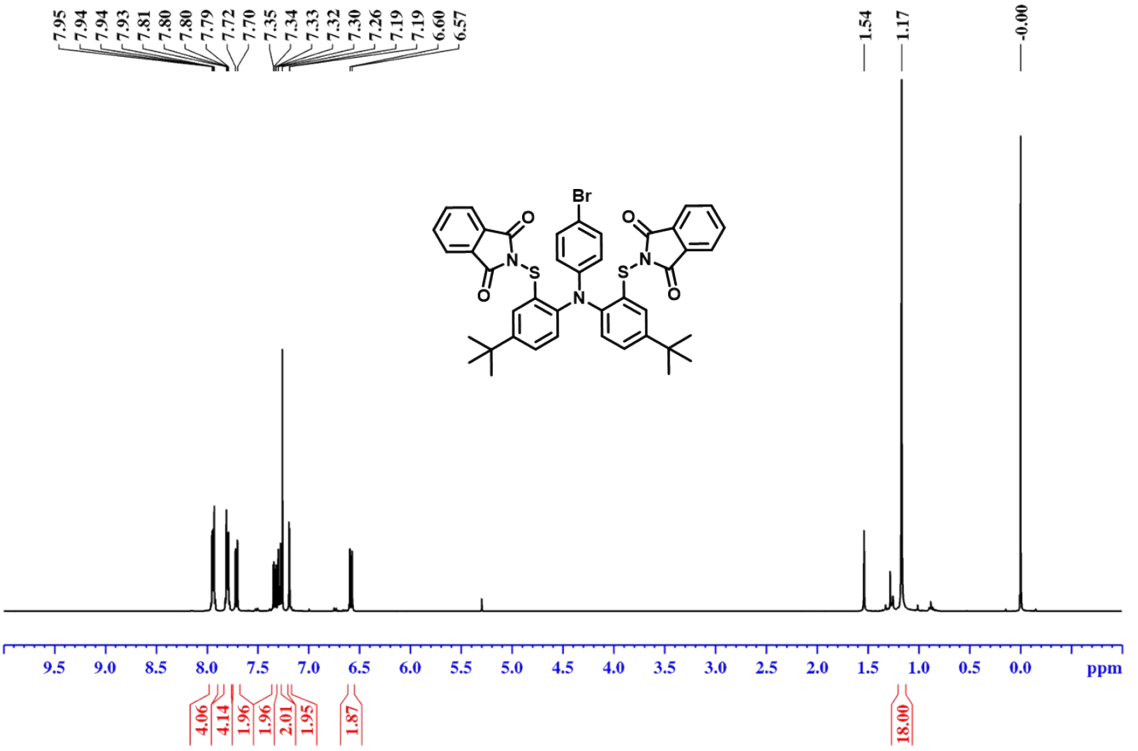
7.95
7.94
7.94
7.93
7.81
7.80
7.80
7.79
7.72
7.70
7.35
7.34
7.33
7.32
7.30
7.26
7.19
7.19
6.60
6.57
1.54
1.17
-0.00
Br
9.5 9.0 8.5 8.0 7.5 7.0 6.5 6.0 5.5 5.0 4.5 4.0 3.5 3.0 2.5 2.0 1.5 1.0 0.5 0.0 ppm
4.06
4.14
1.96
1.96
2.01
1.95
1.87
18.00

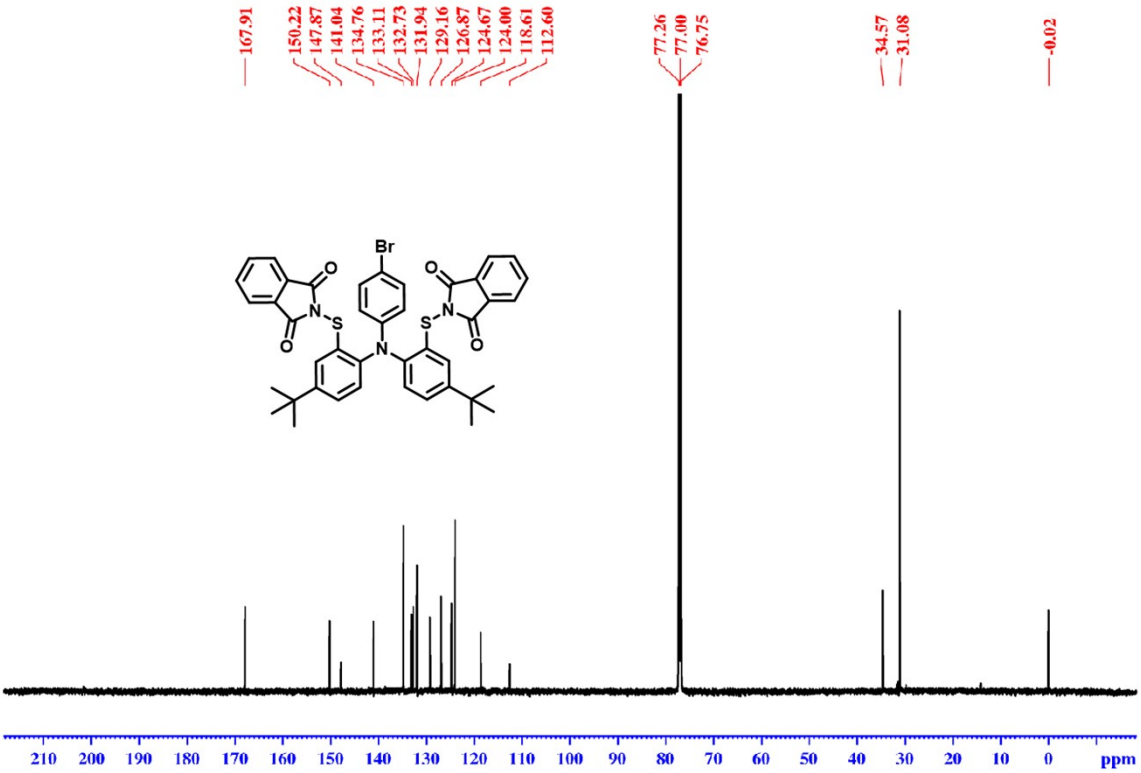
167.91
150.22
147.87
141.04
134.76
133.11
132.73
131.94
129.16
126.87
124.67
124.00
118.61
112.60
77.26
77.00
76.75
34.57
31.08
-0.02
Br
210 200 190 180 170 160 150 140 130 120 110 100 90 80 70 60 50 40 30 20 10 0 ppm

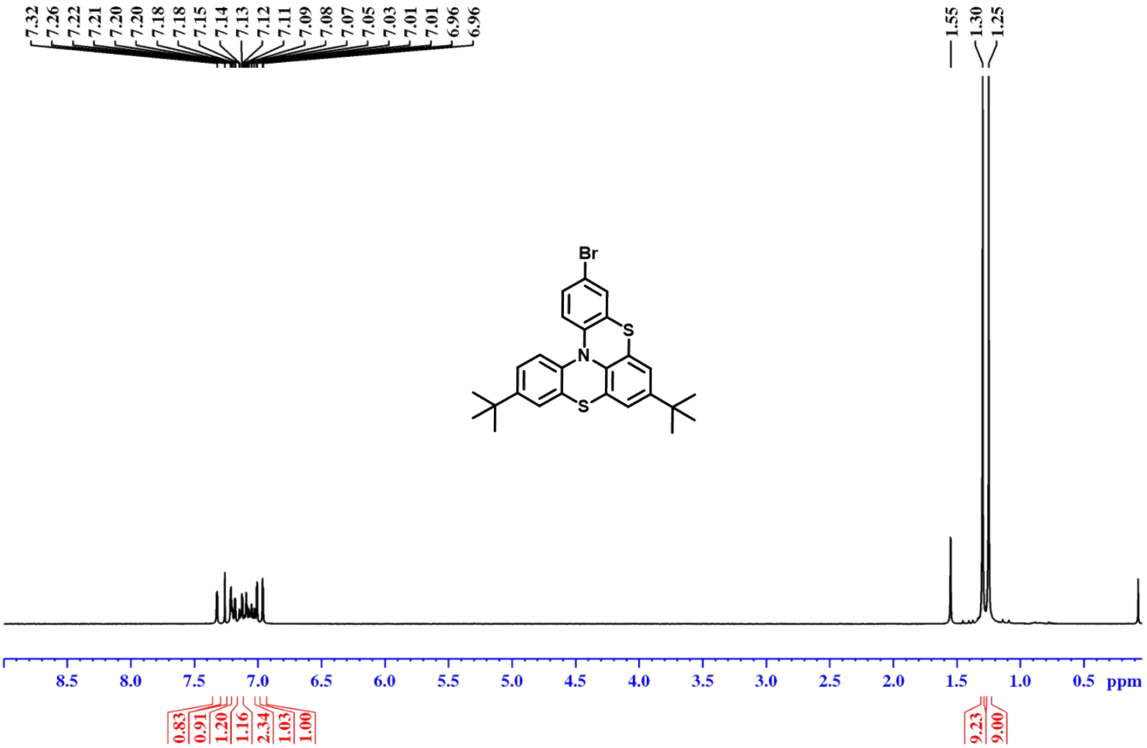
7.32
7.26
7.22
7.21
7.20
7.20
7.18
7.18
7.15
7.14
7.13
7.12
7.11
7.09
7.08
7.07
7.05
7.03
7.01
7.01
6.96
6.96
1.55
1.30
1.25
Br
S
N
S
8.5
8.0
7.5
7.0
6.5
6.0
5.5
5.0
4.5
4.0
3.5
3.0
2.5
2.0
1.5
1.0
0.5
ppm
0.83
0.91
1.20
1.16
2.34
1.03
1.00
9.23
9.00

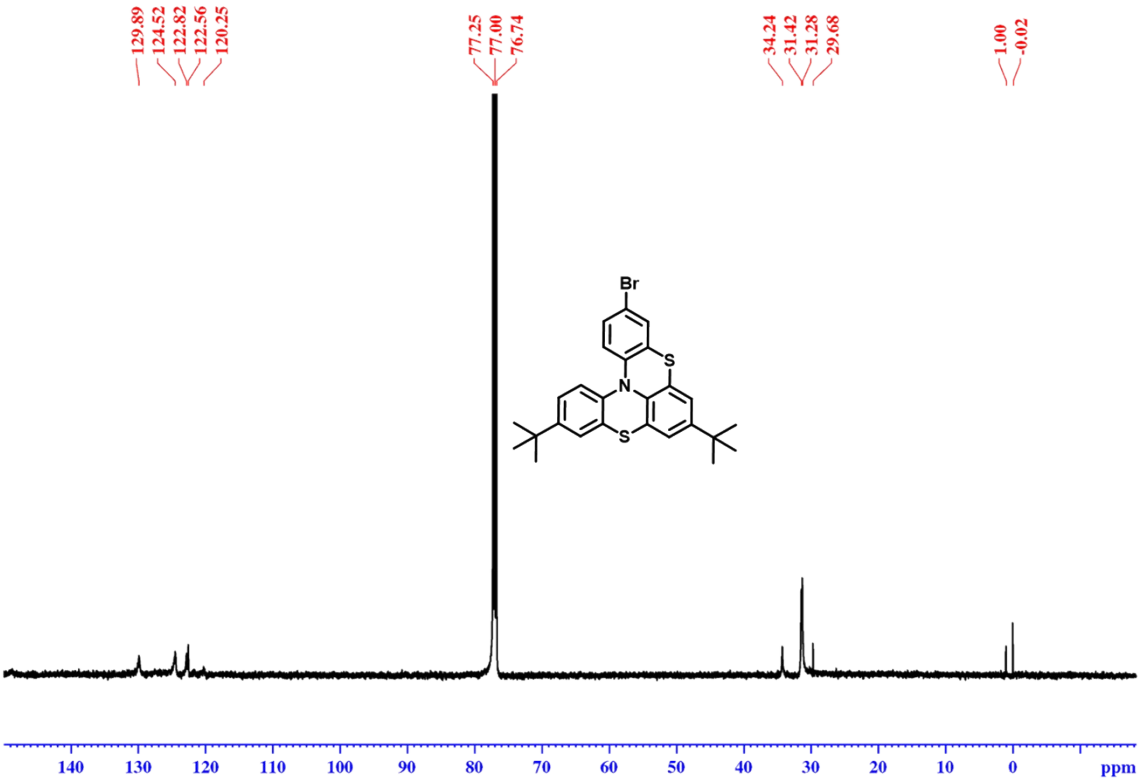
129.89
124.52
122.82
122.56
120.25
77.25
77.00
76.74
34.24
31.42
31.28
29.68
1.00
-0.02
Br
S
N
S
140
130
120
110
100
90
80
70
60
50
40
30
20
10
0
ppm

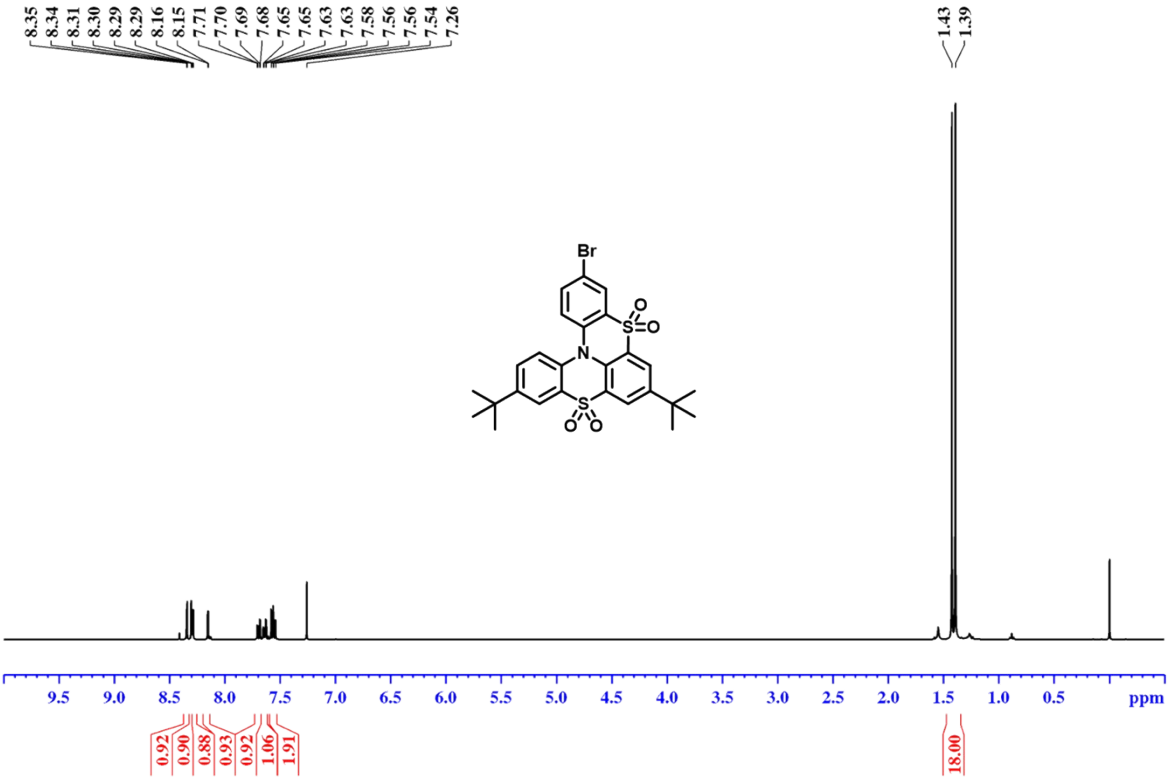
8.35
8.34
8.31
8.30
8.29
8.29
8.16
8.15
7.71
7.70
7.69
7.68
7.65
7.65
7.63
7.63
7.58
7.56
7.56
7.54
7.26
1.43
1.39
Br
O
S
O
N
S
O
O
9.5
9.0
8.5
8.0
7.5
7.0
6.5
6.0
5.5
5.0
4.5
4.0
3.5
3.0
2.5
2.0
1.5
1.0
0.5
ppm
0.92
0.90
0.88
0.93
0.92
1.06
1.91
18.00

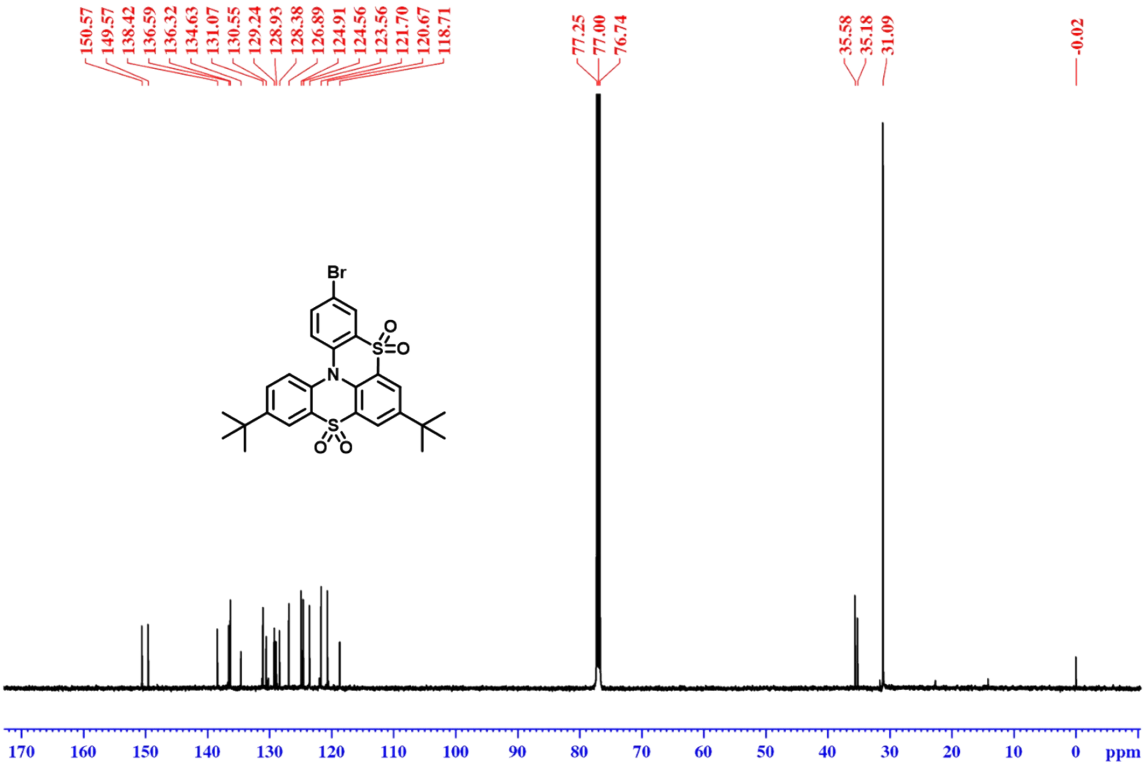
150.57
149.57
138.42
136.59
136.32
134.63
131.07
130.55
129.24
128.93
128.38
126.89
124.91
124.56
123.56
121.70
120.67
118.71
77.25
77.00
76.74
35.58
35.18
31.09
-0.02
Br
O
S
O
N
S
O
O
170
160
150
140
130
120
110
100
90
80
70
60
50
40
30
20
10
0
ppm

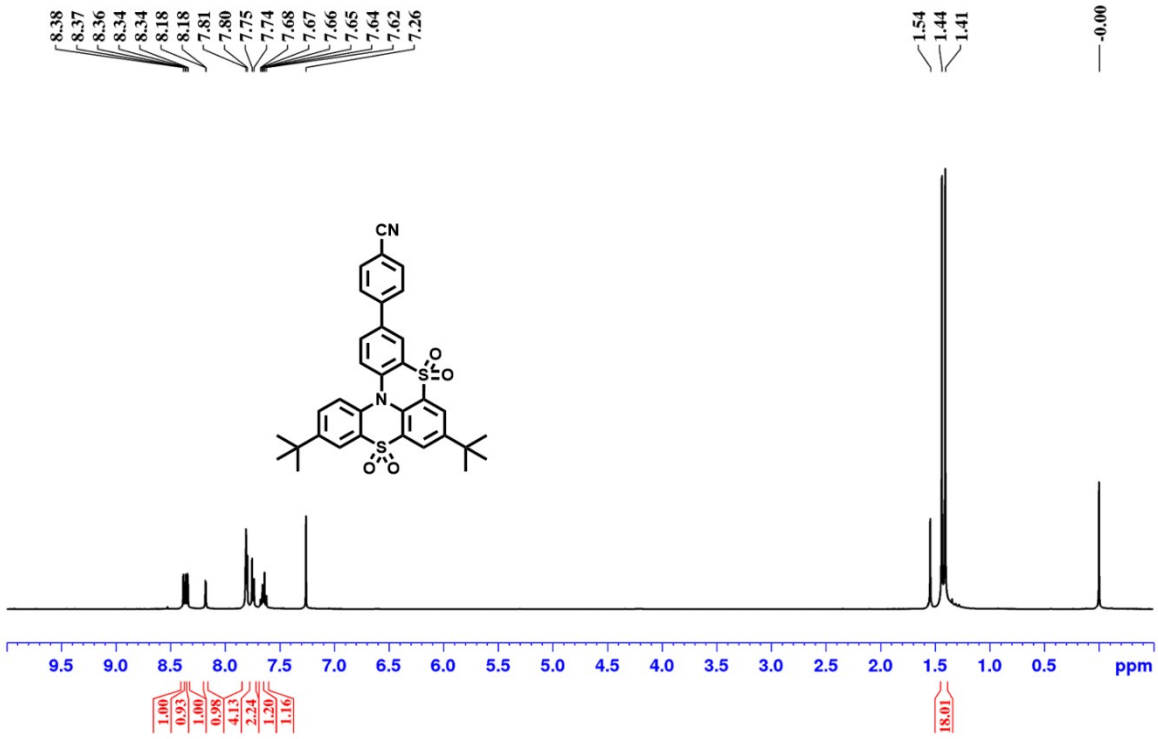
8.38
8.37
8.36
8.34
8.34
8.18
8.18
7.81
7.80
7.75
7.74
7.68
7.67
7.66
7.65
7.64
7.62
7.26
1.54
1.44
1.41
-0.00
CN
O
O
S
N
S
O
O
9.5 9.0 8.5 8.0 7.5 7.0 6.5 6.0 5.5 5.0 4.5 4.0 3.5 3.0 2.5 2.0 1.5 1.0 0.5 ppm
1.00
0.93
1.00
0.98
4.13
2.24
1.20
1.16
18.01

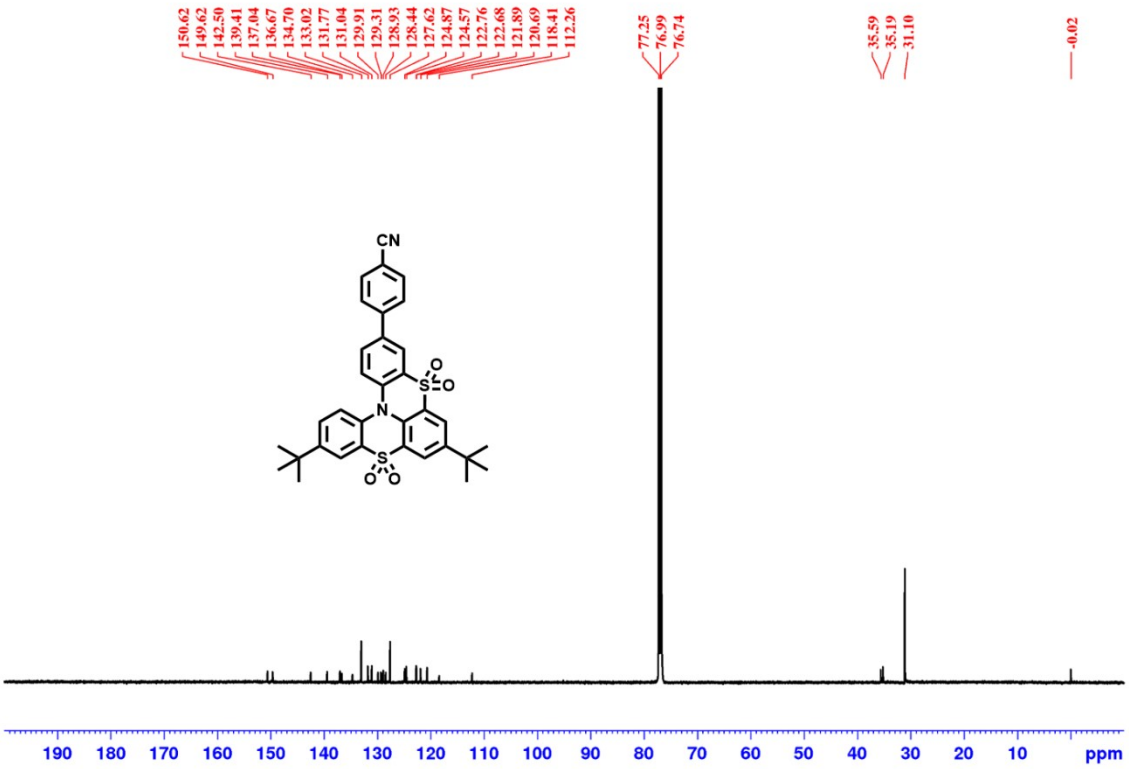
150.62
149.62
142.50
139.41
137.04
136.67
134.70
133.02
131.77
131.04
129.91
129.31
128.93
128.44
127.62
124.87
124.57
122.76
122.68
121.89
120.69
118.41
112.26
77.25
76.99
76.74
35.59
35.19
31.10
-0.02
CN
O
O
S
N
S
O
O
190 180 170 160 150 140 130 120 110 100 90 80 70 60 50 40 30 20 10 ppm

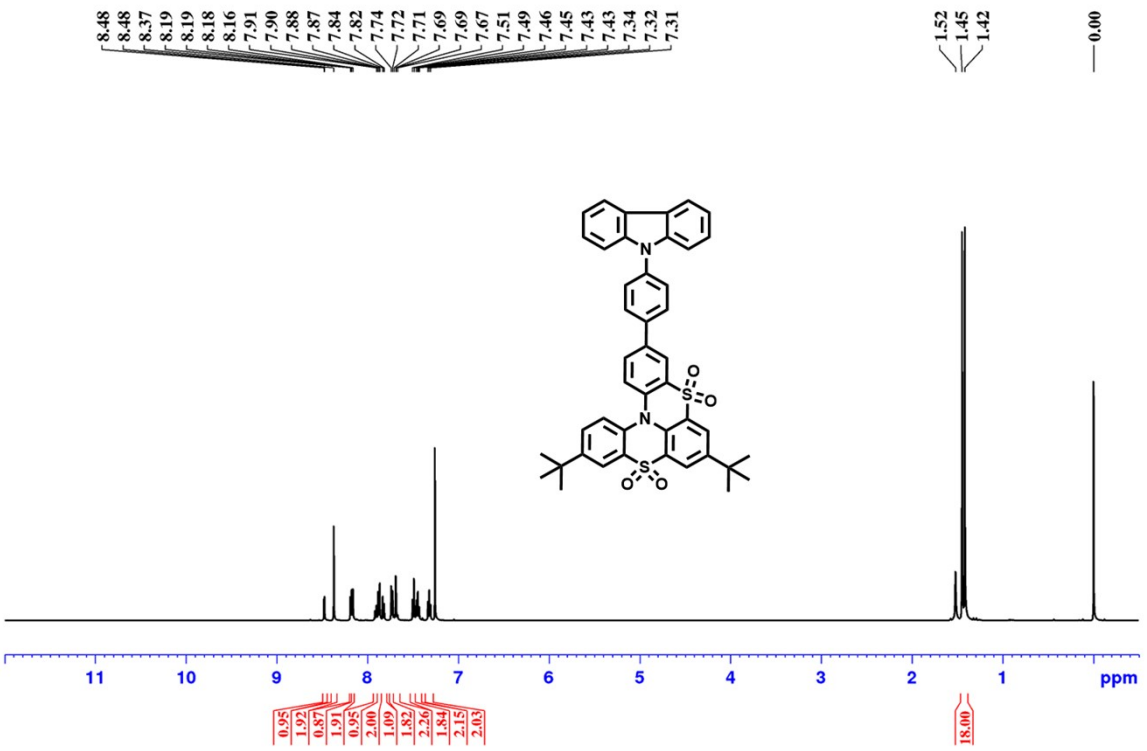
8.48
8.48
8.37
8.19
8.19
8.18
8.16
7.91
7.90
7.88
7.87
7.84
7.82
7.74
7.72
7.71
7.69
7.69
7.67
7.51
7.49
7.46
7.45
7.43
7.43
7.34
7.32
7.31
1.52
1.45
1.42
0.00
11
10
9
8
7
6
5
4
3
2
1
ppm
0.95
1.92
0.87
1.91
0.95
2.00
1.09
1.82
2.26
1.84
2.15
2.03
18.00

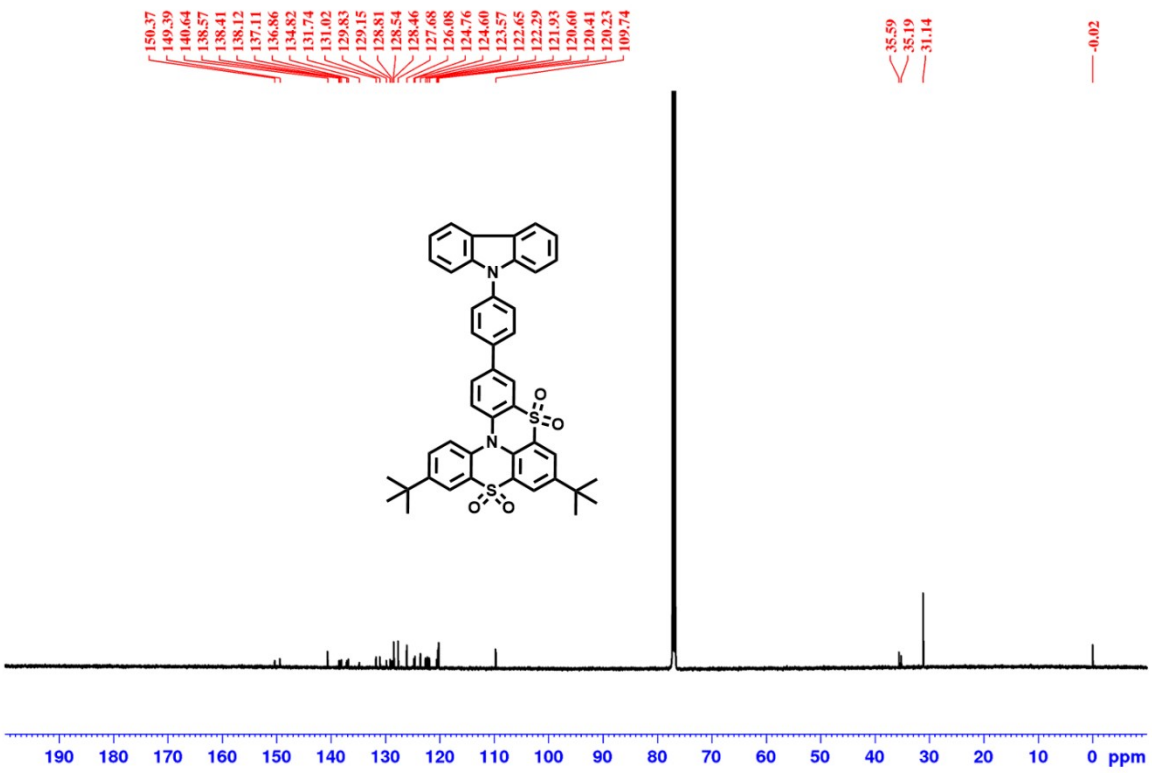
150.37
149.39
140.64
138.57
138.41
138.12
137.11
136.86
134.82
131.74
131.02
129.83
129.15
128.81
128.54
128.46
127.68
126.08
124.76
124.60
123.57
122.65
122.29
121.93
120.60
120.41
120.23
109.74
35.59
35.19
31.14
-0.02
190
180
170
160
150
140
130
120
110
100
90
80
70
60
50
40
30
20
10
0
ppm

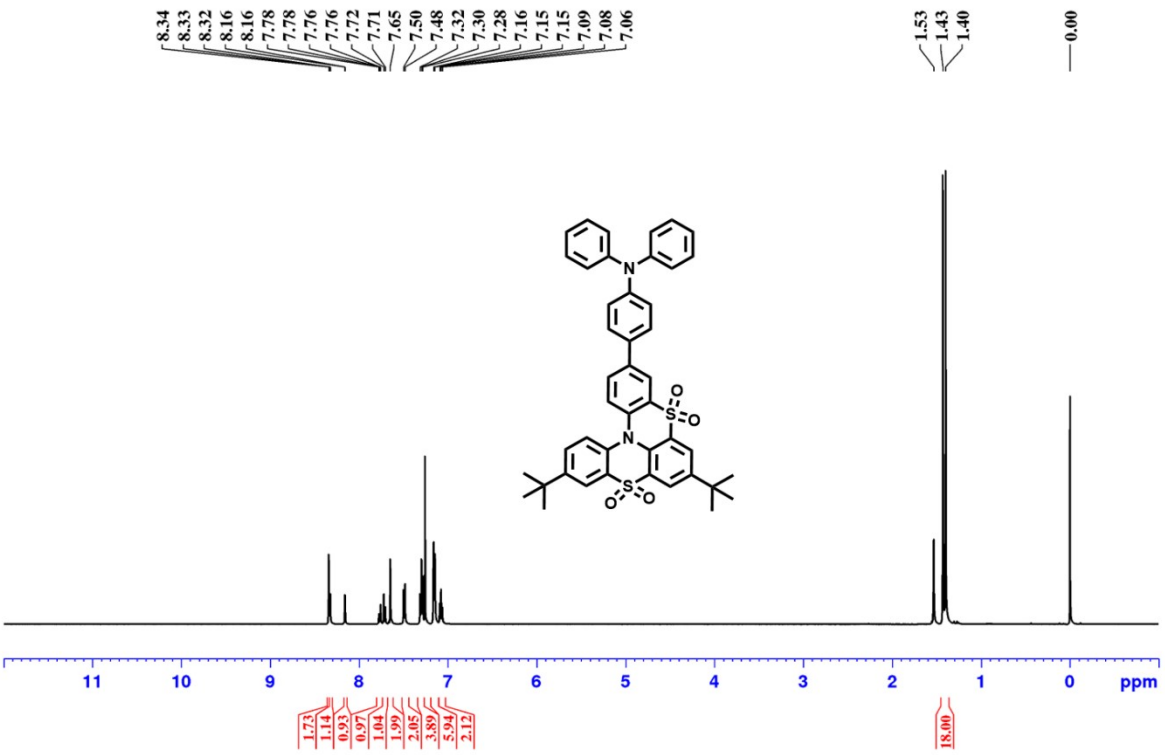
8.34
8.33
8.32
8.16
8.16
7.78
7.78
7.76
7.76
7.72
7.71
7.65
7.50
7.48
7.32
7.30
7.28
7.16
7.15
7.15
7.09
7.08
7.06
1.53
1.43
1.40
0.00
11
10
9
8
7
6
5
4
3
2
1
0
ppm
1.73
1.14
0.93
0.97
1.04
1.99
2.05
3.89
5.94
2.12
18.00

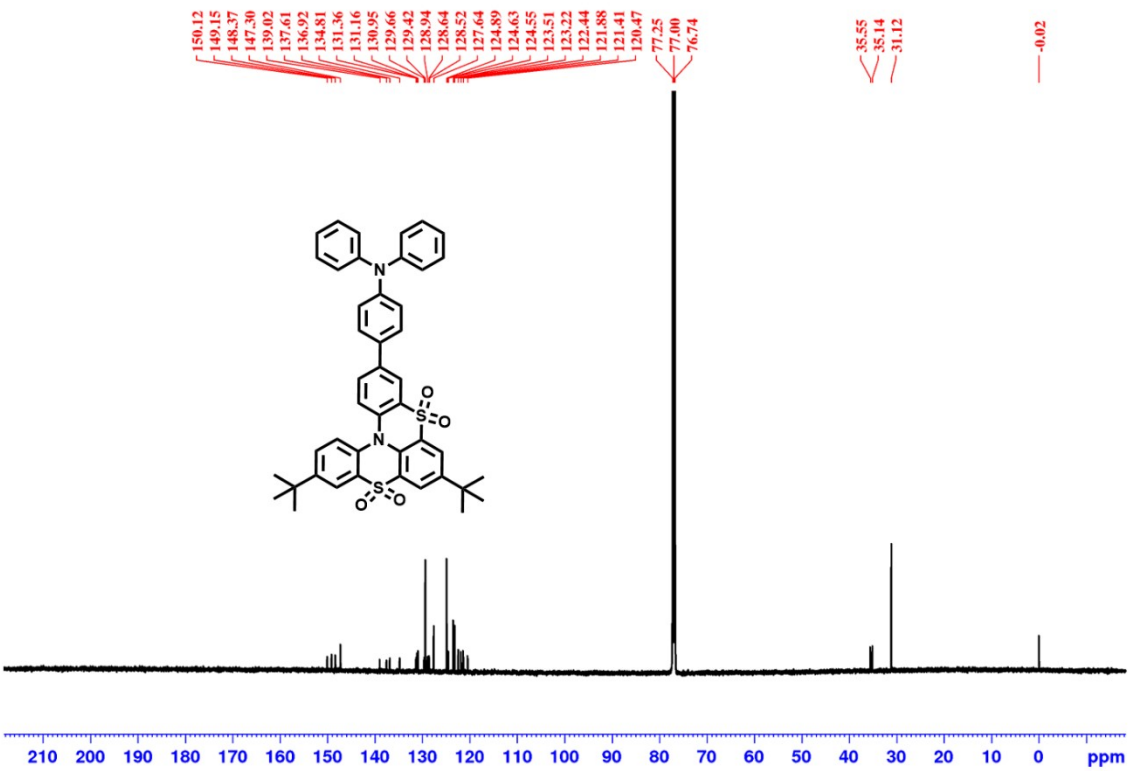
150.12
149.15
148.37
147.30
139.02
137.61
136.92
134.81
131.36
131.16
130.95
129.66
129.42
128.94
128.64
128.52
127.64
124.89
124.63
124.55
123.51
123.22
122.44
121.88
121.41
120.47
77.25
77.00
76.74
35.55
35.14
31.12
-0.02
210
200
190
180
170
160
150
140
130
120
110
100
90
80
70
60
50
40
30
20
10
0
ppm

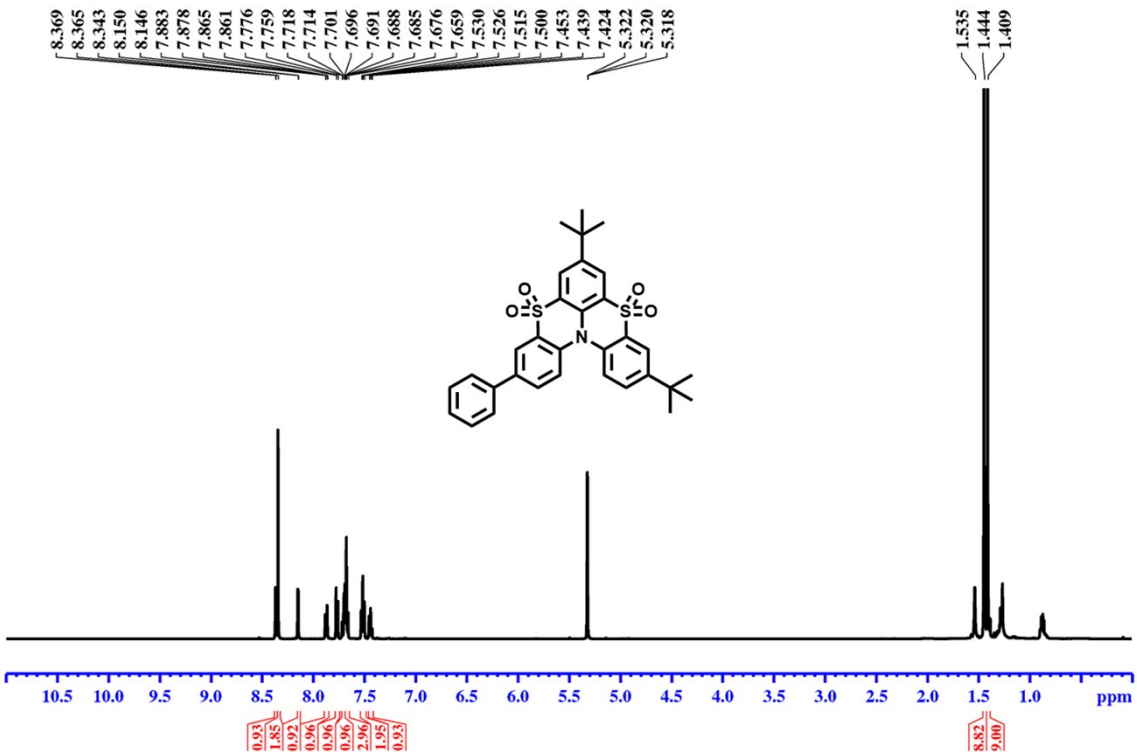
8.369
8.365
8.343
8.150
8.146
7.883
7.878
7.865
7.861
7.776
7.759
7.718
7.714
7.701
7.696
7.691
7.688
7.685
7.676
7.659
7.530
7.526
7.515
7.500
7.453
7.439
7.424
5.322
5.320
5.318
1.535
1.444
1.409
10.5 10.0 9.5 9.0 8.5 8.0 7.5 7.0 6.5 6.0 5.5 5.0 4.5 4.0 3.5 3.0 2.5 2.0 1.5 1.0 ppm
0.93
1.85
0.92
0.96
0.96
0.96
2.96
1.95
0.93
8.82
9.00

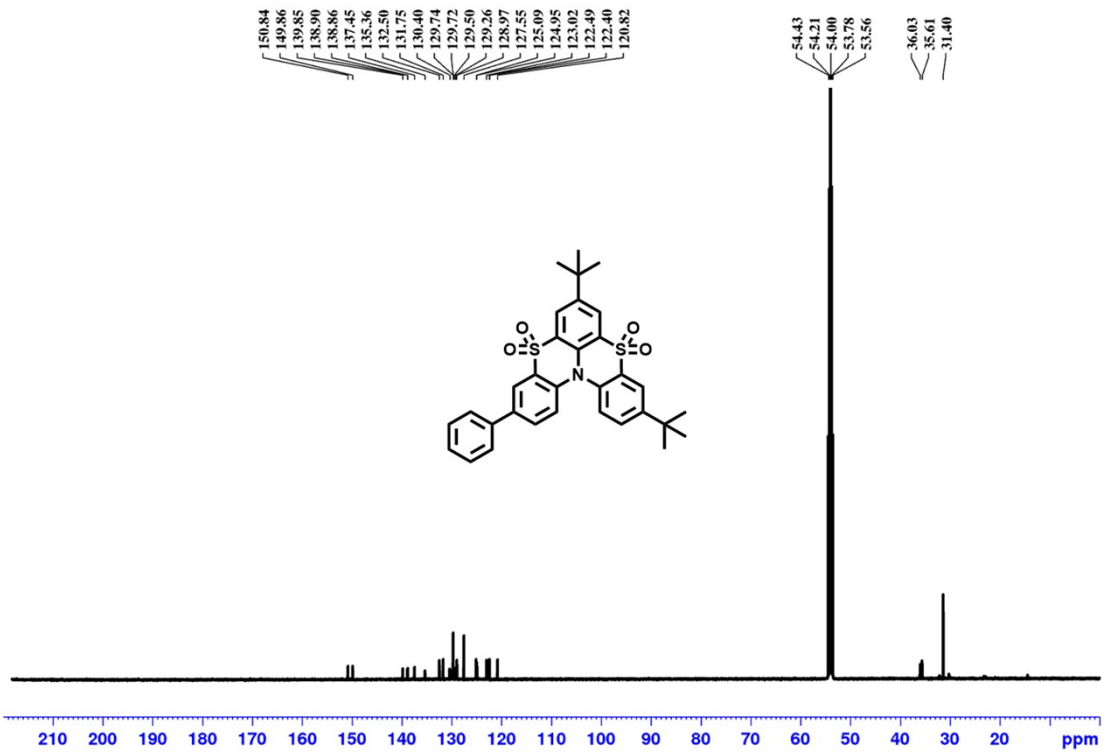
150.84
149.86
139.85
138.90
138.86
137.45
135.36
132.50
131.75
130.40
129.74
129.72
129.50
129.26
128.97
127.55
125.09
124.95
123.02
122.49
122.40
120.82
54.43
54.21
54.00
53.78
53.56
36.03
35.61
31.40
210 200 190 180 170 160 150 140 130 120 110 100 90 80 70 60 50 40 30 20 ppm

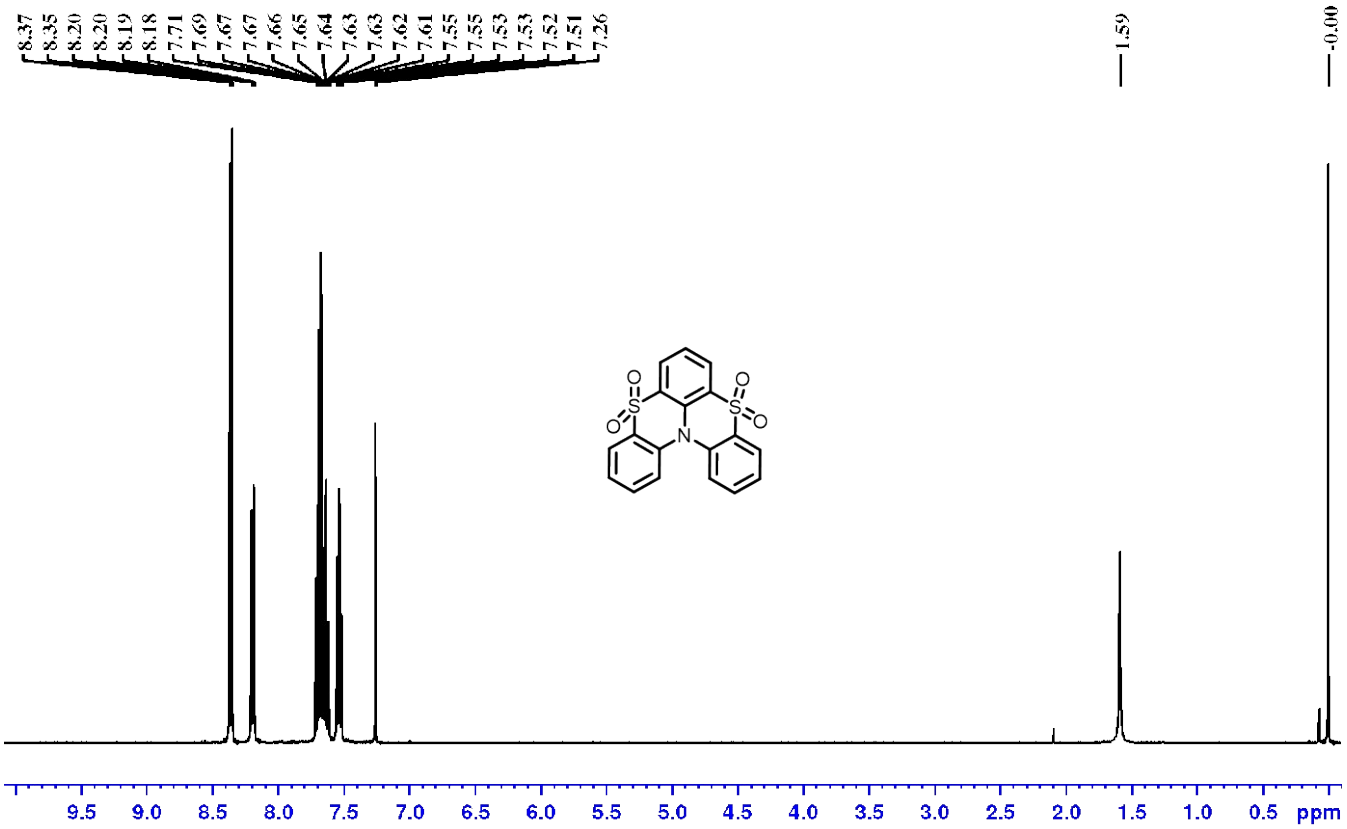
8.37
8.35
8.20
8.20
8.19
8.18
7.71
7.69
7.67
7.67
7.66
7.65
7.64
7.63
7.63
7.62
7.61
7.55
7.55
7.53
7.53
7.52
7.51
7.26
1.59
-0.00
9.5
9.0
8.5
8.0
7.5
7.0
6.5
6.0
5.5
5.0
4.5
4.0
3.5
3.0
2.5
2.0
1.5
1.0
0.5
ppm

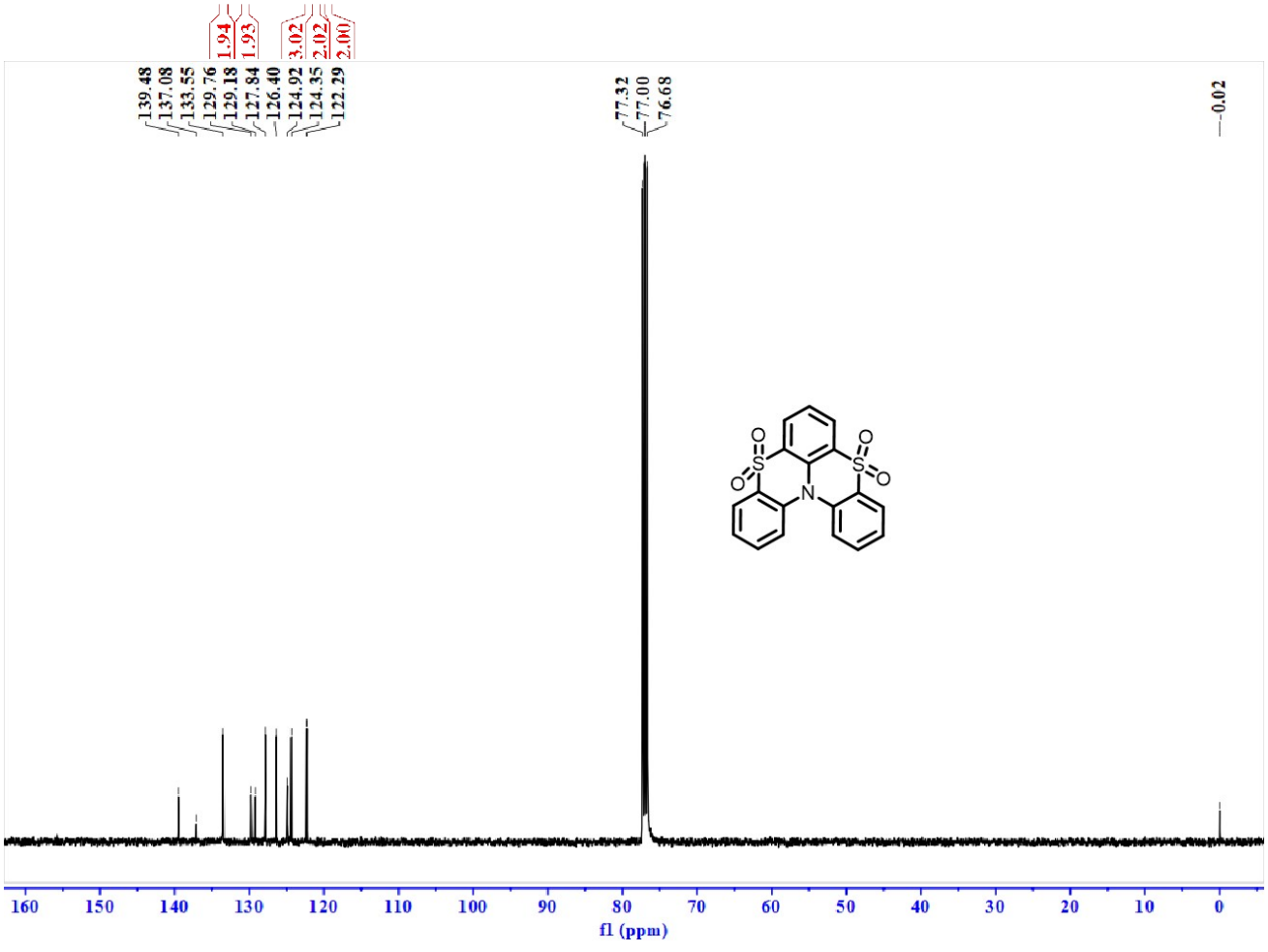
1.94
1.93
3.02
2.02
2.00
139.48
137.08
133.55
129.76
129.18
127.84
126.40
124.92
124.35
122.29
77.32
77.00
76.68
-0.02
160
150
140
130
120
110
100
90
80
70
60
50
40
30
20
10
0
f1 (ppm)